TECHNISCHE UNIVERSITÄT WIEN
Vienna University of Technology

D I P L O M A R B E I T

Role of electrode placement in cochlear implants for fiber excitation according to the tonotopic principle

Ausgeführt am Institut für

ANALYSIS UND SCIENTIFIC COMPUTING
der
TECHNISCHEN UNIVERSITÄT WIEN

unter der Anleitung von

Ao.Univ.Prof. Dipl.-Ing. DDDr. Frank Rattay

durch

Sophia Ulonska, BSc
Ybbsstrasse 5/12, 1020 Wien

Wien, 18. September 2013

Sophia Ulonska

Danksagung

Allen voran möchte ich mich bei meinem Betreuer Professor Rattay für seine freundliche und geduldige Begleitung bedanken. Danke Thomas Potrusil und Cornelia Wenger für Eure Unterstützung und Eure Modelle; sie stellen die Basis dieser Arbeit dar.

Meiner Familie gebührt unendlicher Dank für ihre liebevolle Unterstützung in allen Belangen und während meines ganzen Studiums. Dario, Dir danke ich sehr dafür, dass Du stets für mich da warst.

Abstract

The cochlear implant (CI) is an example for successful functional electrical nerve stimulation. An important CI component is the electrode array implanted in the scala tympani of the cochlea. Usually CIs mimic the tonotopic principle of the cochlea, which means high frequencies lead to a stimulation of basal fibers and low frequencies to a stimulation of apical fibers.

This thesis bases on a computer simulation of the electrical stimulation of the spiral ganglion cells (SGCs) which are the elements of the cochlear nerve. For this model, the cochlear geometry and the pathway of a selection of thirty SGCs were gathered from a μCT of a human cochlea. Also the different conductances of the tissue in the cochlea were considered. The external potential generated by an electrode in the cochlea was computed by applying the FEM; the fibers were modeled by a Hodgkin-Huxley compartment model.

The main topic of this thesis was to focus on the electrical stimulation of apical SGCs. Usually the SGCs are assumed to be more or less planar. However, the apical SGCs described in this thesis show a spirality. For the two most apically arising SGCs this spiral structure is very prominent in the distal axons. Beginning in the apex, several electrodes with a distance of 30° were placed in the cochlea; actually electrode arrays of present CIs don't reach up to the apex of the cochlea.

The spirality in the dendrites of the two most apical SGCs results in a quite low distance towards multiple electrodes along their length - in contrast to the ideal planar SGC, which is only near towards one electrode. Actually the distance towards an electrode and the external potential at this point do not correspond linearly due to the inhomogeneity of the cochlear tissue; but still nearer SGCs are generally stimulated with lower current than SGCs, which are farer away.

So it was investigated, that for electrodes between 720° and 810° and a small range of current it is possible to stimulate simultaneously only the SGC which is actually the closest, as well as one (or both) of the SGCs spiraling in their peripheral axons and coming quite near to the electrode. This means, a subpopulation of tonotopically non-neighboring fibers is stimulated. With other words, the tonotopic principle is disturbed by electrical stimulation of the apex.

Zusammenfassung

Das Cochleaimplantat (CI) ist ein Beispiel für die erfolgreiche funktionelle Elektrostimulation des Hörnervs. Ein wichtiger Bestandteil des CIs ist der Elektrodenträger, der in die Scala Tympani der Cochlea implantiert wird. Gewöhnlicherweise imitieren CIs das tonotopische Prinzip der Cochlea; das heißt, hohe Frequenzen führen zu einer Stimulation von basalen Fasern, niedrige Frequenzen dagegen zu einer Stimulation von apikalen Fasern.

Diese Diplomarbeit basiert auf einer Computersimulation zur Elektrostimulation der Spiralganglionzellen (SGZ) des Hörnervs. In diesem Modell konnte mit Hilfe eines μCT einer menschlichen Cochlea die realistische Geometrie einer Cochlea und der tatsächliche Verlauf einer Auswahl von dreißig SGZ berücksichtigt werden. Auch die verschiedenen Leitfähigkeiten des Gewebes in der Cochlea wurden miteinbezogen. Das durch die Elektroden generierte elektrische Potential wurde mit Hilfe der FEM berechnet; für die Fasern wurde das Hodgkin-Huxley-Kompartment-Modell verwendet.

Der zentrale Aspekt dieser Diplomarbeit war, die elektrische Stimulation der apikalen SGZ zu untersuchen. Normalerweise haben die SGZ in der Cochlea einen planaren Verlauf. Die apikalen SGZ dieses Modells jedoch spiralisieren zum Teil. Hierbei weisen gerade die zwei am weitesten apikal gelegenen SGZ eine deutliche Spiralität in ihren peripheren Axonen auf. Beginnend im Apex wurden einige Elektroden in die Scala Tympani mit einem Abstand von 30° positioniert; Elektrodenträger von heutigen CIs reichen allerdings nicht bis zum Apex.

Die spiralisierenden Dendriten der zwei apikalsten SGZ sorgen dafür, dass diese Fasern entlang ihrer Länge einen relativ geringen Abstand zu mehren Elektroden haben. Ideale planare SGZ dagegen nähern sich nur einer Elektrode an. Auf Grund der Inhomogenität des Gewebes in der Cochlea hängen der Abstand zu einer Elektrode und das elektrische Potential nicht linear zusammen; dennoch sind nähere SGZ in der Regel mit weniger Strom erregbar als weiter entfernte.

Es hat sich herausgestellt, dass es für Elektroden zwischen 720° und 810° in der Cochlea und einem gewissen Strombereich möglich ist, gleichzeitig die eigentlich nächste SGZ und eine (oder beide) der in ihren Dendriten spiralisierenden SGZ anzuregen. Somit werden tonotopisch nicht benachbarte Fasern gleichzeitig stimuliert. In anderen Worten, das tonotopische Prinzip wird bei der Elektrostimulation des Apex der Cochlea verletzt.

Contents

List of Symbols and Glossary

A_n membrane surface of compartment n

C_n membrane capacity of compartment n

E electric field

G_n membrane conductance of compartment n

$I_{ax,n}$ ohmic axial current of compartment n

$I_{cap,n}$ capacitive current of compartment n

$I_{ion,n}$ ion current of compartment n

J current density

$R_n/2$ internal resistance of compartment n to left resp. right hand side

T temperature in °C

V voltage

V_K potassium battery voltage

V_{Na} sodium battery voltage

$V_{e,n}$ external voltage of compartment n

$V_{i,n}$ internal voltage of compartment n

V_{leak} leakage battery voltage

V_{rest} resting potential

Φ potential field

ρ_i internal resistivity

σ electrical conductivity

c_n specific membrane capacitance of compartment n

$g_{K,n}$ constant for maximum potassium conductance per cm^2 of compartment n

$g_{Na,n}$ constant for maximum sodium conductance per cm^2 of compartment n

$g_{leak,n}$ constant for maximum leakage conductance per cm^2 of compartment n

$i_{ion,n}$ ion current density of compartment n

k temperature coefficient with $k = 3^{0.1T-0.63}$

n_{myel} number of myelin layers of a compartment

t time

ANO monophasic anodic pulse with default length of 100μs

BIA biphasic pulse: anodic followed by cathodic pulse, default length of 100μs per phase

BIC biphasic pulse: cathodic followed by anodic pulse, default length of 100μs per phase

CAT monophasic cathodic pulse with default length of 100μs

List of Abbreviations

AP action potential

BM basilar membrane

CI cochlear implant

EAS electric acoustic stimulation

FEM finite element method

IHC inner hair cells

IN internode

IS initiation site

OHC outer hair cells

SGC spiral ganglion cells

SM scala media

ST scala tympani

SV scala vestibuli

TH threshold

TP tonotopic principle

Chapter 1

Introduction

Nowadays computer simulations are an important tool in medical research. When the model is valid, for example investigating the consequences of changing parameters of the model can be performed relatively quick and cheap. Furthermore, for instance ethically arguable and costly animal experiments can be avoided to some extent.

This thesis describes a model of the electrical stimulation of the spiral ganglion cells (SGC) in the cochlea. The technical application of this is the cochlear implant (CI). This is a device with the aim to stimulate auditory neurons, which are still functional but cannot be stimulated the natural way. For this an electrode array is implanted in the scala tympani of the cochlea. More information on it, considering components and technique as well as performance of CIs, is given in chapter 2.

The model consists of two parts: first of all the potential distribution in the cochlea generated by the electrodes of the CI has to be computed; afterwards the response of the neuron fibers towards this electrical stimulation is calculated. The first part of the model was performed by applying the finite element method (FEM) in COMSOL; it was developed by T. Potrusil at the IBK Innsbruck. The mathematical background is described in more detail in chapter 3.1, whereas the configuration and parameters of the model are given in 4. The part of the neuronal response is performed in MATLAB and bases on a model given by C. Wenger in [Wenger, 2012]; for this the neurons were modeled by the Hodgkin-Huxley compartment model, which is presented in chapter 3.2. More information on the concrete configuration of the implementation and the parameters of the model are given in chapter 5.

A validation of the model, especially treating the case of changing the values of the electrical conductivity of the different materials of the cochlea, is given in chapter 6; there it is also presented how distance of the fibers towards the electrodes, the external

potential along the neuron lengths and the excitability of the fibers correspond.

The peculiarity of the described model is, that it considers the realistic geometry of a given cochlea; furthermore the realistic pathway of a selection of thirty SGCs was provided. So neither the cochlear geometry nor the pathway of the SGC is idealized. It turned out, that the apical SGCs are partially spiraling, see chapter 7; whereas usually all SGC are assumed to be more or less planar. To find out the consequences of the spiraling shape, several electrodes with a distance of 30° were placed in the cochlea, beginning in the apex. Present CIs are not implanted so deep in the cochlea, but in a computer simulation this is possible. In chapter 8 it was investigated what effect the spirality of the fibers has on their electrical excitability. Because of the high spirality in the dendrites of some apical fibers, these fibers come quite near to many electrodes along their length. It turned out, that this can result in a simultaneous stimulation of non-neighboring subpopulations of fibers for several electrodes, hence the tonotopic principle is violated.

Finally in chapter 9 a discussion about the correctness of the model and the described consequences of the spirality is given.

Chapter 2

Short introduction to cochlear implants

The cochlear implant (CI) is a prosthetic device, which allows patients suffering from a complete or partial sensorineural hearing loss to recover auditory sensations and even the possibility of understanding speech. The CI is implanted in the cochlea and it's strategy is to stimulate the auditory nerve electrically.

There is a lot of literature concerning CIs. Extensive reviews on them are given for example by [Wilson and Dorman, 2008a], [Wilson and Dorman, 2008b] and [Zeng et al., 2008]. These reviews act as a base for this chapter, which gives a short introduction to CIs, and the chapter's structure follows theirs to some extent.

After an introduction to normal hearing and electrical stimulation of a deafened ear, the components and the basic technique of CIs are presented. Afterwards more attention is given to explaining the various possible processing strategies. It is followed by a section treating the intracochlear electrode array by mentioning it's materials and stimulation types. Finally present and future performance of CIs is the topic: after a review about the performance of CIs nowadays, a perspective is presented, how CIs could be improved in future.

2.1 Normal hearing and electrical stimulation

In normal hearing, sound waves first pass the outer ear: they are collected by the pinna, follow the auditory canal and finally reach the tympanic membrane. The middle ear - consisting of this tympanic membrane (the ear drum) and the auditory ossicles malleus, incus and stapes - has the function of an acousto-mechanical coupling of the sound waves and an amplification of the signal, and finally leads it to the round window of the

cochlea. This causes a movement of the fluids inside the cochlea - and therefore of the basilar membrane (BM). This membrane has special properties: from base to apex it's stiffness decreases and it's width increases. This leads to the effect, that it is resonant to high frequencies in the base and to low frequencies in the apex. This spatial distribution of the signal's frequencies is the tonotopic principle (TP).

The hair cells on the organ of Corti sense the movement (of the liquids and the BM) in their environment. These cells in the cochlea are essential for hearing and there are two types of them: three rows of outer hair cells (OHC) and one row of inner hair cells (IHC) along the length of the cochlea. Their function is the following: the OHCs act as amplifiers and improve the hearing resolution - destruction of them worsens hearing; whereas the IHCs have the function to stimulate chemically their corresponding auditory neurons (the SGC) by causing action potentials (APs) at the peripheral ends, which travel along the fiber up to the brain.

However, there are various reasons for disturbing this pathway and leading to deafness. E.g. there are multiple ways to impair the sensitive hair cells, whereas not necessarily all hair cells are destroyed. Besides diseases or drugs, there is also a noise-induced damage of hair cells; other reasons are aging or genetically caused [Wilson and Dorman, 2008a].

Besides having damaged hair cells, frequently also several neurons are at least partially damaged [Zimmermann et al., 1995], [Hinojosa and Marion, 1983]. However, when the neurons are not missing completely, auditory sensations can be recovered by electrical stimulation. For this, electrodes are implanted in the inner ear, which are activated corresponding to the specific pattern of stimulation. The resulting electric potential leads to hyper- and depolarizations along the nerve; and to APs when the stimulus is high enough. In general an AP does not start at the peripheral end like in normal hearing, but somewhere at the dendrite, axon or at the soma, this also depends on the distance to the electrode or the stimulus type [Javel and Shepherd, 2000],[Rattay et al., 2001a].

2.2 Components and basic technique of a cochlear implant

CIs consist of several components. For example [Wilson, 2004] and [Zeng et al., 2008] give broad overviews over the aspects concerning the elements of CIs.

As illustrated in figure 2.1, for most implants the system is built up as follows: there are external components like the behind the ear (BTE) housing (consisting of a microphone, batteries and a speech processor) and the external transmitter; internal components are an implanted receiver and stimulator, when required a reference electrode (in case of monopolar stimulation) and the intracochlear electrode array implanted in the

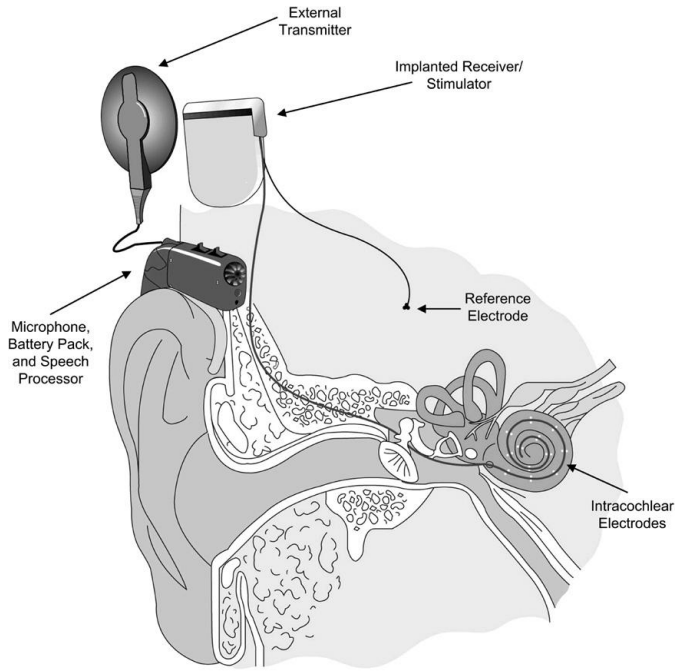

Figure 2.1: Illustration of the components of a cochlear implant [Wilson and Dorman, 2008b].

scala tympani (ST) of the cochlea.

The course from sound to an auditory signal when using a CI is in short words the following: the microphone collects the sound and amplifies it; this signal acts as an input for the speech processor, which converts it into a pattern of stimulating pulses via a specific processing strategy. The next step is the transmitter. It consists of a coil and sends power and stimulation information to the internal receiver - also a coil - via radio frequency. The incoming signal is decoded and the stimulator sends a pattern of stimulating pulses to the electrodes. The stimulation generally follows the tonotopic principle: high frequencies in the sound lead to a stimulation of electrodes in the basal part, whereas low frequencies provoke a stimulation of apical electrodes [Wilson and Dorman, 2008a].

Some people have residual hearing for low frequencies due to remaining functional apical hair cells. In this case, the idea is to stimulate electrically the basal (and mid) part of the cochlea, whereas the apical part is stimulated acoustically. This special type of stimulation is called EAS (electric acoustic stimulation). Such devices are basically a combination of a CI and a hearing aid, this means a combination of electrical and acoustical stimulation.

Although a CI is in general built up as described, there are slight differences among the products of various manufacturers. For example they differ in input dynamic range,

data transmission, processing strategy or electrode array design. Generally the performance of different systems is comparable, but there can be significant differences between them, as for example noted in [Lazard et al., 2012] or [Spahr et al., 2007]; see also section 2.5.

2.3 Processing strategies of cochlear implants

Advances in processing strategies enhanced the quality of CIs tremendously. This paragraph overviews several established and still researched strategies.

For a better understanding, first of all a short explanation for the envelope and the fine structure of a signal is given: by decomposing a band-passed signal by the Hilbert transform, one can describe an analytic signal by a term including the coarse, slowly varying envelope $A(t)$ of the signal and the quickly varying fine structure $\psi(t)$:

$$Y(t) = A(t)\exp[i\psi(t)]. \tag{2.1}$$

As an example, fig. 2.2 shows a signal, it's envelope $A(t)$ and it's fine structure $\psi(t)$. The fine structure can also be interpreted by the zero-crossings of the original waveform.

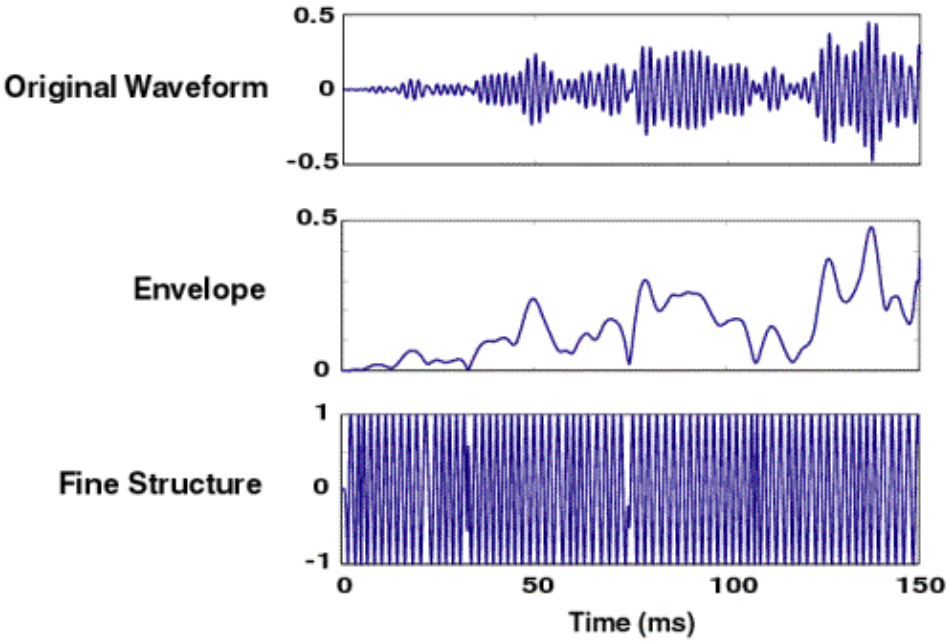

Figure 2.2: Illustration of the envelope and fine structure of a signal. Taken from `http://research.meei.harvard.edu/Chimera/motivation.html`; accessed on 27. June 2013.

Initially processing strategies mainly focused on the coarse envelope, but nowadays spectral and temporal fine structure get more attention. As described by [Smith et al., 2002], the coarse envelope contains enough information for the perception of speech. However, the fine structure is relevant for localization of sound as well as pitch and therefore e.g. for music perception. This explains why - as presented in more detail in section 2.5 - speech understanding on non-tonal languages works quite well nowadays, while perception of tonal languages like mandarin (in which pitch is of high importance) or of music still needs to be improved. However, even in strategies focusing on the coarse envelope at least some fine structure is contained [Wilson and Dorman, 2008a].

In the following, several established processing strategies dealing with coarse information are explained. Furthermore a description of recently used and still researched strategies focusing on fine information is given. The description mainly follows [Zeng et al., 2008].

Strategies based upon the temporal envelope of a signal are widely spread. A famous representative is the CIS strategy (continuous-interleave-sampling) by [Wilson et al., 1991], which is also the basis of n-of-m strategies like SPEAK or ACE. The CIS strategy works as follows: the sound is collected by the microphone and comes to a pre-amplifier. Afterwards, there is a specific number of bandpass filters. The number depends on the system (more precisely on the number of electrodes of the device). Now for each channel the temporal envelope is computed, for example by full-wave rectification or a Hilbert transform [Zeng et al., 2008]. Afterwards the signal needs to be compressed non-linearly, since the the amplitudes vary a lot in nature. Then for each pathway the signal is modulated and biphasic pulses are sent to the electrodes. Mimicking the tonotopic principle, for low frequencies signals are sent to apical electrodes and for high frequencies to basal electrodes. The pulse rates are about or even higher than 1000 pulses per second per electrode [Wilson and Dorman, 2008b]. One important aspect is, that the stimulation of the electrodes is not simultaneous. This is to avoid an accumulation of electric fields [Wilson and Dorman, 2008a].

Similar strategies to CIS are the strategies n-of-m, SPEAK (spectral peak) or ACE (advanced combination encoder). The difference of these strategies to CIS is, that when m is the overall number of channels (and electrodes), after the envelope computation only n channels with highest amplitude are selected. The strategies n-of-m, SPEAK and ACE differ in whether the number n is fixed or not and in the stimulation rate [Wilson and Dorman, 2008b].

As already noted, the trend nowadays is to take account of the fine structure of the signal, whereas some strategies focus on the spectral, others on the temporal fine structure. Actually this means that more information is transmitted, which leads to a requirement of more independent electrodes. However, since developing arrays with more electrodes is complicated, new processing strategies are developed [Zeng et al., 2008]. Two examples are described in the following.

One example for representing the spectral fine structure is using virtual channels

(also called current steering)[Wilson and Dorman, 2008a]. The concept is to generate multiple stimulation sites between a limited number of electrodes by simultaneous stimulation of (neighboring) electrodes, while the pulse amplitude and polarity might differ. In this strategy the accumulation of electric fields is intended. For example, a virtual channel between two electrodes can be generated by stimulating both electrodes with half of their pulse amplitude. The aim is a maximum between both electrodes.

Another representative is the fine structure processing strategy (FSP) by MED-EL [Hochmair et al., 2006]. It combines temporal and spatial fine structure. For the temporal fine structure, the two to three most apical electrodes are stimulated by CSSS (Channel-Specific Sampling Sequences), which focuses on the temporal fine structure. So the stimulation starts, when there is a zero-crossing in the fine structure. Furthermore the temporal fine structure is processed by virtual channels, although here the stimulation is sequentially and not simultaneously.

2.4 The electrode array: material, implantation and stimulation configuration

As noted above, the electrode array of a CI is directly implanted in the ST of the cochlea. The electrodes then stimulate the auditory neurons, whereas the type of stimulation depends on the applied processing strategy as described in the previous section 2.3.

In general the electrode array consists of a carrier made of a silicon rubber with micro electrodes made of platinum-iridium alloy on it [Zeng et al., 2008]. The concrete layout differs for the manufacturing companies. Often the array is straight yet flexible, like FLEX^{SOFT} by MED-EL, but it can also be pre-folded like Contour Advance™ by Cochlear®.

Nowadays CIs are usually 18-26 mm long in comparison to the cochlear length of 35 mm, further insertion is hard due to the coiling and since the cochlea gets narrower up to the apex [Wilson and Dorman, 2008a]. It seems to improve speech understanding, when the apical part of the cochlea is also stimulated [Hochmair et al., 2003]. However, a further insertion depth can cause more trauma [Adunka and Kiefer, 2006]. Nonetheless, later in this thesis (in chapter 4) electrodes are presented, that are placed very apical on positions, which could not be reached with nowadays designs and insertion techniques.

An aim in placing the electrode carrier is to keep the distance between nerve and electrodes small. This is possible by locating the implant at the inner wall of the ST nearer to the modiolus. However, only few implants follow this strategy. These are called perimodiolar arrays and are often pre-folded like the Contour Advance™ array. These arrays might reduce channel interactions (caused by the overlapping of the electric fields) but do not necessarily improve speech perception [Hughes and Abbas, 2006].

The number of electrodes varies for the designs; it is for example 22 in the Con-

tour Advance™ device. As described above, the tonotopic principle is mimicked. This means, that the basal electrodes are stimulated for high frequencies and apical electrodes for low frequencies. The aim is, that an electrode is associated with a specific subpopulation of neurons, that should not be overlapping. However, one has to note, that the ST is filled with perilymph, a liquid of high conductivity. This leads to the effect, that the target regions of the electrodes might overlap. Therefore nowadays only four to eight electrodes can act independently at the same time [Wilson and Dorman, 2008a] - a diminutive number in comparison to about 3500 inner hair cells [Ashmore, 2008].

There are multiple stimulation configurations, for example monopolar, bipolar or tripolar. In a monopolar configuration a remote (reference) electrode outside of the cochlea (e.g. in the temporalis muscle) is needed. In the bipolar mode one has a pair of neighboring intracochlear electrodes, in which one acts as active electrode and the other as return electrode. For a tripolar configuration, two neighbors of the active electrode act as return electrodes, whereas the return current is split up equally [Zeng, 2004]. Monopolar stimulation has lower activation thresholds than bipolar [Pfingst and Xu, 2004] and tripolar configuration [Snyder et al., 2008]. Hence the monpolar stimulation is preferred nowadays over the bipolar configuration [Wilson and Dorman, 2008b].

Furthermore, stimulus rate, length and the sequence of cathodic and anodic pulses depend on the processing strategy. However, the stimulus amplitudes are patient specific, since an individual tuning is needed to stimulate only certain subpopulations of neurons.

2.5 Performance of nowadays CIs and perspective on improving strategies

After this introduction to the technical aspects, now the topic is discussed, how good CIs work. Can a few electrodes really replace the function of the about 3500 hair cells? Therefore in the following the state of the art in performance of CIs is shortly overviewed. Afterwards some concepts are presented, how CIs could be improved in future.

State of the art in performance

Good news are, that for many patients speech recognition in a quiet environment works quite well with current CIs. However, noisy conditions reduce the recognition ability. The nowadays average score for sentence recognition is about over 70 % correct in quiet environment. There are even patients with great scores: [Wilson and Dorman, 2007] report on a subject with scores of almost 100 % correct in monosyllabic words and sentence recognition in quiet environment. Even in noisy conditions this patient scored

over 70 % correct. However, most patients do not have such an excellent restoration of hearing. Unfortunately some patients profit hardly from their implant and do poorly.

The presented studies mainly base on data for non-tonal languages like English. However, an interesting aspect is, that due to an insufficient pitch representation, a correct recognition of tonal languages like Mandarin is harder than in normal hearing [Wei et al., 2004]. Furthermore, of course hearing is not only about understanding sentences or words: unfortunately the identification of melodies is hard, even for top scorers [Wilson and Dorman, 2008b]. The same holds for emotion detection [Luo et al., 2007]. As noted in section 2.3, all this is might due to an insufficient representation of the signal's fine structure: [Smith et al., 2002] show, that the fine structure is important for recognition of pitch or melodies. It seems that speech perception in noisy conditions and music perception is improved with processing strategies considering fine structure [Vermeire et al., 2010], [Lorens et al., 2010]. This is also confirmed by the following aspect: as reported above, patients with residual hearing in the apical region can get an EAS implant. They seem to benefit from this: they have better hearing in noisy conditions and better melody recognition [Gantz et al., 2005]. The reason could be, that especially in the apical region fine structure is transmitted via phase locking.

It is sure, that different designs and technologies can influence the efficiency of CIs. So [Lazard et al., 2012] report significant differences in performance between brands. They noted these differences especially in a quiet environment and to a lower extent in noisy conditions. [Spahr et al., 2007] as well see differences between different manufacturers, but they observed more differences in harder hearing situations like a noisy environment.

A further interesting aspect is, that the duration of wearing a CI has a significant positive influence on the performance. The effect is the strongest in the first year, but even holds up to at least 3.5 years after implantation [Blamey et al., 2012]. This can be interpreted as learning and confirms the assumption, that the auditory cortex is meaningful for performance [Wilson and Dorman, 2008a].

Furthermore, having detected a severe to profound hearing loss, one probably should not wait too long before implanting a CI: the duration of this hearing loss before an implantation of a CI negatively affects performance and even lessens the positive effects of learning reported above [Blamey et al., 2012].

Perspective on possible performance improvement

There are several ideas and efforts for improving CIs. [Wilson and Dorman, 2008b] present a long list of ideas, like improving processing strategies, reducing the distance between electrodes and neurons or promoting training of the patients. Several aspects are explained shortly in the following.

One idea is to think about alternatives to electrical stimulation. An example for this is optical stimulation via infrared radiation [Izzo et al., 2007]. This procedure is able to

provoke a highly spatial selective stimulation. The mechanism is based on the effect, that infrared radiation causes a heating and therefore changes the electrical capacitance of the target neurons [Shapiro et al., 2012]. However, this strategy still is quite experimentally.

Another approach is to improve processing strategies, e.g. by focussing more on the fine structure which is of importance for pitch or music recognition as mentioned above. Also lower distance between electrodes and neurons could lead to better results. The distance could be reduced via two ways: on the one hand, one can focus on the design of the electrode array like perimodiolar arrays and on improving the insertion of this array. Another idea is to let the neurons grow towards the electrodes.

Furthermore, beside these efforts for bringing forward the technique of CIs, one should not disregard appropriate training of the patients. It can help patients with very poor results, but also patients with high scores can profit by special trainings e.g. in difficult hearing situations like a noisy environment [Fu and Galvin III, 2008].

Summing up these ideas, future patients surely will profit from further research and the experience of involved people like designers or surgeons. However, also present patients might have the chance to improve their hearing ability by a customized training.

Chapter 3

Mathematical background: Volume conductor and compartment modelling

Later in this thesis, a model is presented, that computes the reactions of neurons towards electrodes in a realistic cochlea. The concrete implantation of this model is described in chapter 4 and 5. However, here the mathematical background of the simulation is explained.

The simulation consists of two parts: first of all the potential distribution in the cochlea generated by the electrodes is computed. This is done by solving the equations of the volume conductor model, which are described in the following, by the finite element method (FEM). Afterwards the reaction of neurons towards this potential is calculated with a neuron model; in our case it is a compartment model with Hodgkin-Huxley dynamics. In the following, the equations of the volume conductor model and the compartment model are explained separately.

3.1 Volume conductor model

It is assumed to have a domain Ω consisting of inhomogeneous tissue and a stimulating electrode inside of Ω. Furthermore a grounding is defined, this could be a return electrode or - as in our case - the outer boundary of Ω. It is assumed, that the generated current flows through the passively conducting, surrounding tissue in all three dimensions. This means, the tissue acts as a volume conductor [Plonsey, 2000]. The aim is to compute the distribution of the potential field Φ in the domain Ω.

The tissue is assumed to be biological; when further having frequencies under 1

kHz one can assume quasi-static conditions [Plonsey, 2000]. This allows considerable simplifications - so the impact of capacity, induction or propagation can be disregarded - and to perform a stationary study [Roth, 2000]. However, e.g. [Bossetti et al., 2008] note, that one should be aware, that this assumption was not made for neural stimulation (where frequencies might are above 1 kHz) but applications like EEG, EMG etc. Therefore they compared the potential of a quasi-static and a exact solution of the Helmholtz equation in a homogeneous medium. They came to the conclusion, that quasi-static conditions still can be applied - however, under specific conditions like not too short pulse rates (e.g. of about $100\mu s$) and proper conductivity values. This shall act as an justification for assuming quasi-static conditions in the following; but one should have in mind, that it is a simplification.

The equations for the volume conductor model assuming quasi-static conditions are as follows: it holds, that the electric field E is the gradient of the potential field Φ:

$$E = -\nabla\Phi. \tag{3.1}$$

Furthermore Ohm's law with an active current source is

$$J = \sigma E + J_i \tag{3.2}$$

with J as current density and J_i as the current density generated by the current source; σ is the electrical conductivity. With quasi-static conditions we have zero divergence of J, which leads to to

$$\nabla \cdot J = \nabla \cdot \sigma E + \nabla \cdot J_i = 0. \tag{3.3}$$

So with eq. 3.1 we have

$$\nabla \cdot J_i = -\nabla \cdot \sigma E = \nabla \cdot \sigma(\nabla\Phi) = \sigma\Delta\Phi. \tag{3.4}$$

This leads to the Poisson equation

$$\sigma\Delta\Phi = -I_{sv} \tag{3.5}$$

where we have I_{sv} as the internal volumetric current source per unit volume. Further explanation of the volume conductor model is for example given in [Klepfer et al., 1997].

Additionally one has to state initial values and boundary conditions: so we assume $V_0 = 0$ V except for the boundary of the active electrode, where we have $V_0 = 1$ V. Furthermore, a grounding has to be defined. At the boundary of the outer geometry $\partial\Omega$ Neumann boundary conditions are stated:

$$-n \cdot J = 0. \tag{3.6}$$

3.2 Mathematical neuron model

For modeling the neurons in this thesis, a compartment model with Hodgkin-Huxley channel kinetics is considered. The original Hodgkin-Huxley model [Hodgkin and Huxley, 1952] acts as basis for many neuron models. Their model originates from experiments with an unmyelinated squid axon. However, it can be adapted to human neurons by a compartment model.

The following presents the differential equation of the compartment model as well as important parameters; it mainly bases on [Rattay et al., 2003]. The concrete values of parameter values are given later (in chapter 5) in table 5.1 and 5.2.

Compartment model: differential equation

The SGCs are bipolar, so they only have one dendrite and one axon. They are given by a compartment model. This means, a neuron is interpreted by an electrical network consisting of several connected subunits like the soma, pre- and postsomatic compartments and axonal and dendritic nodes of Ranvier and internodes. A part of this network is shown in figure 3.1.

For every compartment n a specific membrane conductance G_n, a membrane capacity C_n and an internal resistance to left and right $R_n/2$ are given. Furthermore, we have an internal and an external voltage $V_{i,n}$ and $V_{e,n}$. Additional compartment-specific parameters are the membrane surface A_n and the number of myelin layers n_{myel}.

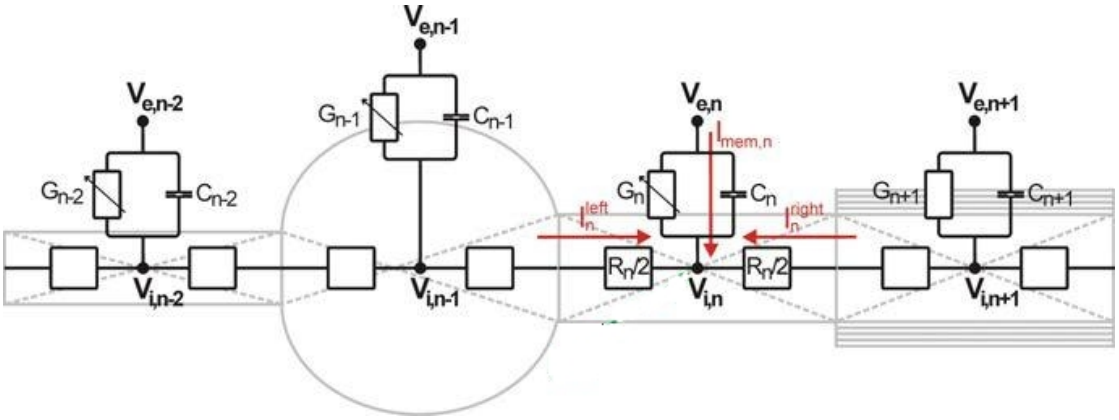

Figure 3.1: Diagram of a part of the electric network of the modeled neuron, showing the soma, the pre- and postsomatic compartments and one internode. Slightly adapted from [Wenger, 2012].

We have to assume several currents at the central point of compartment n: first of all the capacitive current $I_{cap,n}$ and the ion current $I_{ion,n}$ which goes across the mem-

brane. There is furthermore the ohmic axial current $I_{ax,n}$ consisting of the currents to the neighboring compartments. According to Kirchhoff's law, the sum of all currents at a node is zero. So we have

$$I_{cap,n} + I_{ion,n} + I_{ax,n} = 0 \tag{3.7}$$

for every compartment n. Note that $V_{i,n}$ and $V_{e,n}$ as well as the currents $I_{cap,n}$, $I_{ion,n}$ and $I_{ax,n}$ depend on time. The capacitive current is given by

$$I_{cap,n} = \frac{d(V_{i,n} - V_{e,n})}{dt} C_n. \tag{3.8}$$

Furthermore, the axial current can be derived by adding the currents to the left and right side and holds as

$$I_{ax,n} = \frac{V_{i,n} - V_{i,n-1}}{R_n/2 - R_{n-1}/2} + \frac{V_{i,n} - V_{i,n+1}}{R_n/2 - R_{n+1}/2} \tag{3.9}$$

for compartments with two neighbors. Compartments with only one neighbor (namely the first and last compartment) have a reduced form with only one summand.

For simplifying the equations, we state the voltage V being

$$V = V_i - V_e - V_{rest} \tag{3.10}$$

with the resting potential V_{rest}, see tab. 5.2.

Combining all the information leads to a system of differential equations for the rate of voltage change under external stimulation. For (a middle) compartment n one gets the equation

$$\begin{aligned} \frac{dV_n}{dt} = [-I_{\text{ion},n} &+ \frac{V_{n-1} - V_n}{R_{n-1}/2 + R_n/2} + \frac{V_{n+1} - V_n}{R_{n+1}/2 + R_n/2} \\ &+ \frac{V_{e,n-1} - V_{e,n}}{R_{n-1}/2 + R_n/2} + \frac{V_{e,n+1} - V_{e,n}}{R_{n+1}/2 + R_n/2}]/C_n. \end{aligned} \tag{3.11}$$

The reduced differential equations for the first and last compartment hold as

$$\frac{dV_1}{dt} = [-I_{\text{ion},n} + \frac{V_2 - V_1}{R_2/2 + R_1/2} + \frac{V_{e,2} - V_{e,1}}{R_2/2 + R_1/2}]/C_n, \tag{3.12}$$

respectively

$$\frac{dV_{end}}{dt} = [-I_{\text{ion},n} + \frac{V_{\text{end-1}} - V_{\text{end}}}{R_{\text{end}-1}/2 + R_{\text{end}}/2} + \frac{V_{e,\text{end-1}} - V_{e,\text{end}}}{R_{\text{end}-1}/2 + R_{\text{end}}/2}]/C_n. \tag{3.13}$$

The following two paragraphs explain at first the ion current, which is of Hodgkin-Huxley channel kinetics. Afterwards the compartment depending capacity C_n, the membrane surface A_n and the internal resistance R_n are explained.

Hodgkin-Huxley channel kinetics

As mentioned, the kinetics of the ion channels follow [Hodgkin and Huxley, 1952]. Generally one can divide between active and passive compartments. The corresponding parameters further differ for the specific compartments. In active compartments, like the soma, the nodes of Ranvier and the pre- and postsomatic compartments, one assumes the ion current consisting of potassium, sodium and leakage current; whereas for passive compartments like the internodes the ion current only consists of leakage current. Generally the ion current for an active compartment is given by

$$\begin{aligned} I_{\text{ion},n} =& A_n \cdot i_{\text{ion},n} \\ =& A_n(i_{\text{Na},n} + i_{\text{K},n} + i_{\text{leak},n}) \\ =& A(g_{\text{Na},n} m^3 h(V - V_{\text{Na}}) - g_{\text{K},n} n^4 (V - V_{\text{K}}) - g_{\text{leak},n}(V - V_{\text{leak}})). \end{aligned} \tag{3.14}$$

V_{Na}, V_K and V_{leak} are battery voltages; A_n is the compartment surface and $i_{ion,n}$ the current density of the compartment. The parameters $g_{Na,n}$, $g_{K,n}$ and $g_{leak,n}$ are constants for the maximum conductance per cm^2. Note that $g_{leak,n}$ depends on the number of myelin layers of the specific compartment: it is is inversely proportional to the number of myelin layers $n_{myel,n}$. For the concrete values of the parameters see tables 5.1 and 5.2.

The functions m, n, h are interpreted as probabilities (and therefore only have values between 0 and 1) depending on time, which lower the maximum sodium and potassium conductance. They also depend on temperature. Their time derivatives follow equations 3.15a to 3.15c:

$$\frac{dm}{dt} = [-(\alpha_m + \beta_m)m + \alpha_m]k, \tag{3.15a}$$

$$\frac{dh}{dt} = [-(\alpha_h + \beta_h)h + \alpha_h]k, \tag{3.15b}$$

$$\frac{dn}{dt} = [-(\alpha_n + \beta_n)n + \alpha_n]k. \tag{3.15c}$$

One states k as a temperature coefficient. The original squid axon experiment by [Hodgkin and Huxley, 1952] was performed at temperatures of $T = 6.3$°C. To be able to adapt the equations for higher temperatures (especially to take the accelerated gating into account), one sets $k = 3^{0.1T-0.63}$.

The initial values of m, h, n are like

$$m(0) = \frac{\alpha_m(0)}{\alpha_m(0) + \beta_m(0)}, \tag{3.16a}$$

$$h(0) = \frac{\alpha_h(0)}{\alpha_h(0) + \beta_h(0)}, \tag{3.16b}$$

and

$$n(0) = \frac{\alpha_n(0)}{\alpha_n(0) + \beta_n(0)}. \tag{3.16c}$$

The variables α and β depend on voltage and follow the equations 3.17a to 3.17f:

$$\alpha_m = \frac{2.5 - 0.1V}{\exp(2.5 - 0.1V) - 1}, \tag{3.17a}$$

$$\alpha_h = 0.07 \exp(-V/20), \tag{3.17b}$$

$$\alpha_n = \frac{0.1 - 0.01V}{\exp(1 - 0.1V) - 1}, \tag{3.17c}$$

$$\beta_m = 4 \exp(-V/18), \tag{3.17d}$$

$$\beta_h = \frac{1}{\exp(3 - 0.1V) + 1}, \tag{3.17e}$$

$$\beta_n = 0.125 \exp(-V/80). \tag{3.17f}$$

For passive compartments no potassium and sodium current is assumed. So we we have

$$I_{\text{ion},n} = A_n g_{\text{leak},n}(V - V_{\text{leak}}). \tag{3.18}$$

Definition of membrane capacitance C_n, membrane surface A_n and internal resistance R_n

Except for the soma, which is modeled as a sphere, all compartments are modeled as cylinders. This paragraph states the equations for the membrane capacitance C_n, the membrane surface A_n and the internal resistance $R_n/2$ between the center and the left respectively right border of the compartment.

The membrane capacitance C_n depends on the membrane surface and the number of myelin layers $n_{myel,n}$. It is given by

$$C_n = A_n c_n / n_{myel,n} \tag{3.19}$$

with c_n as the specific membrane capacitance (see table 5.2).

The membrane surface of the cylindrical compartments is defined by the lateral surface of the cylinder (without top and bottom) and holds as

$$A_n = d_n \pi \Delta x_n, \tag{3.20}$$

with diameter d_n and length Δx_n (given in table 5.1). The membrane surface of the soma, which is a sphere of radius r, is more complicated, since one also considers the neighboring compartments. Let the diameters of the neighboring compartments be $d_{\text{process},j}$ with $j = 1, 2$; then the membrane surface of the soma is

$$A_{\text{soma}} = 4r^2\pi - \sum(2r\pi h_j) \tag{3.21}$$

with

$$h_j = r - z_j \tag{3.22}$$

and

$$z_j = \sqrt{r^2 - (d_{\text{process},j}/2)^2}. \tag{3.23}$$

The resistance $R_n/2$ between center and border of the compartment to left respectively right side is depends on the internal resistivity ρ_i (see table 5.2) and is

$$R_n/2 = 2\rho_i \Delta x_n/(d_n^2\pi) \tag{3.24}$$

for cylindrical compartments. For the spherical soma we have

$$R_{\text{soma}}/2 = \frac{\rho_i}{2r\pi} \ln \frac{r + z_j}{r - z_j}. \tag{3.25}$$

Chapter 4

Implementation in Comsol

The model, which computes the electrical stimulation of realistic fibers in a realistic cochlear geometry, consists of two parts: the calculation of the potential distribution in the cochlea generated by stimulating electrodes and the computation of the neural response towards it. This chapter describes, how the voltage distribution in the cochlea was obtained. The modeling of the neural response is presented in the following chapter 5.

In short, the calculation was performed the following way: given was a realistic representation of the cochlea as well as stimulating electrodes and a grounding; after defining boundary conditions, material values and physical equations (see chapter 3.1) and meshing the geometry, the voltage distribution was computed by applying the FEM. All this was realized in COMSOL Multiphysics 4.2[1].

In the following, these steps are presented in more detail. First of all, the geometry of the model is explained, considering the creation of a model based on a realistic cochlea in general and the concrete configuration of our model. Afterwards material values, physics, mesh and solution of the model are presented. This is finally followed by a paragraph about the current on the stimulating electrodes.

4.1 Geometry building

The geometry of the model is composed of the cochlea (consisting of the different scalae, outer bone and the modiolus), surrounding tissue and electrodes. After an intro-

[1]Registered trademark of COMSOLAB.

duction how the geometry of a realistic cochlea can be obtained, the concrete configuration of the geometry of the model and the electrode positions are explained.

From the cochlea to a model

When creating a model of a cochlea based on a realistic organ, one has to be aware of the fact, that every cochlea is unique. For example the possible length of a human cochlea ranges widely from about 3.2 to 4.2 cm [Rask-Andersen et al., 2012]. Furthermore the cochlear length is usually shorter for females than for males [Sato et al., 1991]. Besides this, the number of turns of the cochlea is highly varying: often there are assumed to be 2.5 turns; however, even be up to three turns are possible [Biedron et al., 2009],[Tian et al., 2006]. Other differences occur e.g. in the diameters of the cochlear canal [Ketten et al., 1998]. Of course, alongside these striking differences, there are small deviations between various cochleae in the actual shape of the outer bone of the cochlea or the different scalae.

Considering these differences makes it necessary to admit, that results obtained from a model with the geometry of a specific cochlea can not be generalized absolutely to other cochleae. However, even creating a model with average geometric measurements (which would be quite complex and elaborate) would not solve this problem. Furthermore, the advantage of considering a non idealized geometry would be lost.

The geometry of a realistic specimen can be obtained for example by scanning a prepared cochlea with a μCT. This technique works like an usual CT but has a higher resolution. Afterwards the different components of the geometry (outer bone, the scalae etc.) can be gathered by segmenting the achieved images.

For the creation of the geometry of the model described in this thesis, this method was applied to a given cochlea at the Medical University of Innsbruck by T. Potrusil. The isotropic resolution was 3 μm. The gained geometry of the outer bone, scala tympani, scala media and scala vestibuli is presented in fig. 4.1.

Concrete configuration of the geometry in COMSOL

The cochlear geometry gained as described in the previous paragraph, was imported to a COMSOL model. The final geometry in COMSOL was also created by T. Potrusil and consisted of a box containing the cochlea. The cochlea was given by its components scala tympani (ST), scala media (SM), scala vestibuli (SV) and the outer bone; furthermore a modiolus component was considered. Additionally electrodes (defined as spheres) could be placed in the ST of the cochlea. The overall geometry, as it is given in COMSOL, is presented in fig. 4.2.

Note, that in contrast to the model given in [Rattay et al., 2001b] the nerve, the Reissner membrane, the basilar membrane and the organ of Corti were not considered. It would surely present more realistic results and might should be taken in account into

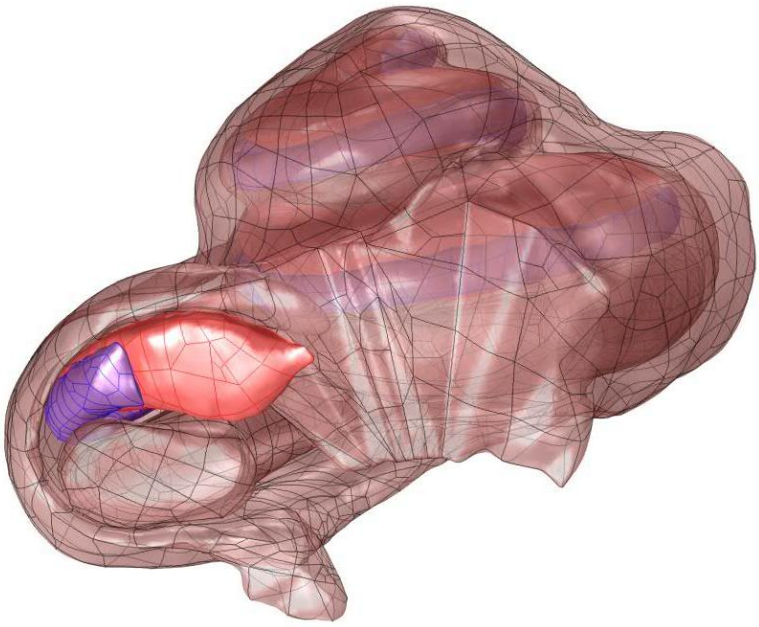

Figure 4.1: Representation of the cochlear geometry. Image provided by T. Potrusil.

future models, but they were neglected to simplify the model. Furthermore the membranes are very thin, which might acts as a justification for disregarding them. Note, that also a silicone carrier (where usually the electrodes are embedded, as described in chapter 2.4) was neglected for reasons of simplification.

The outer box had the function to model the surrounding tissue. Of course this is a great simplification of the tissue around the cochlea. Furthermore size and position of the block are rather arbitrary; instead of a box also a sphere or any other geometry would be possible.

Since the potential distribution caused by a stimulating electrode should be computed, a grounding had to be set: it is possible to place a return electrode somewhere in the box. However, as for example done in [Rattay et al., 2001b], it is also possible to define (parts of) the surface of the surrounding box as grounding. So in the described model the outer surface of the box was defined as the grounding.

Positions of the electrodes

One option for setting the stimulating electrodes in the geometry is to find positions, where the electrodes would be placed, when using realistic electrode arrays of CIs. Though, for this thesis another approach is used: the idea was to place electrodes in

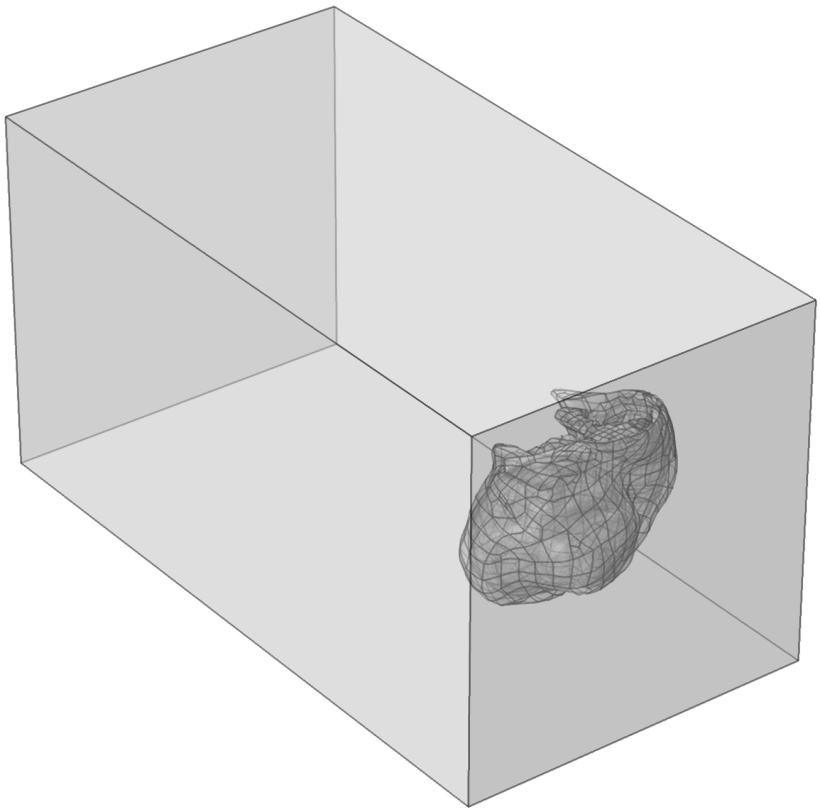

Figure 4.2: Configuration of the overall geometry in COMSOL.

the apical region, to find out what effect electrodes in this region might have. However, the positions of these electrodes could not be reached with nowadays electrode designs: these are usually much shorter than the cochlear length, see chapter 2.4. Hence these positions are purely theoretically on state of the art.

The position finding of the apical electrodes was as follows: beginning in the apex, twelve apical electrodes were set with a distance of 30° referring to the theoretical axis of the cochlea: the midmodiolar axis.

This axis was derived the following way: the apical nerve fibers have a spiraling form, see chapter 7.1. One can assume them to spiral around the midmodiolar axis. Hence this axis was derived mathematically by finding a line with minimum mean square orthogonal distance towards the fibers. This is a rather simple and rough, but time saving approach.

The zero-degrees-plane was defined as the plane, which contains the midmodiolar axis and passes roughly the middle of the beginning entry of the cochlea. Consequently it follows a common definition of the zero-degrees-plane as presented in [Skinner et al., 2007]. Referring to this zero-degrees-plane, successively further five planes were created. These also contained the midmodiolar axis and had a distance of 30° towards the previous plane. Afterwards, starting with an electrode in the uppermost region of the ST, consecutively further eleven electrodes were placed in the ST with their centers on the planes. This means, the electrodes were placed between 570° and 900° of the cochlea. The radius of the electrodes was set to $r = 0.1$mm, except for the most apical electrode in the ST. In order to respect the boundary of the ST its radius was halved to $r = 0.05$mm. In the following, the electrodes are named as EL1 to EL12, beginning at the apex (at 900°).

4.2 Material values

The geometric components of the model are the surrounding tissue, the outer cochlear bone, the three scalae SM, SV and ST, the modiolus and the electrodes. They all have different assigned material values. For example the scalae are filled with a liquid of high conductivity, whereas the outer bone has a high resistivity.

Such as the main geometry, the material values and assignments were supplied by T. Potrusil. The required parameters were electrical conductivity σ and relative permittivity, whereas the conductivity values (except for the modiolus) follow the values presented in [Rattay et al., 2001b], which base on [Finley et al., 1990] and [Kosterich et al., 1983].

Both ST and SV are cavities filled with the liquid perilymph, the SM is filled with endolymph. The material bone was assigned to the outer bone of the cochlea as well as to the surrounding tissue. Actually, the surrounding tissue could have other material values, but the choice fell on taking the same as the outer bone of the cochlea. The modiolus was assumed to be of a tissue consisting of bone and nerve tissue. Therefore it's material value is between bone and nerve and a material denoted as 'bone-nerve' was assigned to it. The concrete values are given in table 4.1.

The influence of the relative permittivity is rather marginal. However, the electrical conductivity is is more relevant. Hence, in chapter 6.1 the sensitivity of the model towards changes of the electrical conductivity is evaluated.

4.3 Physics, mesh and solution

As physics the predefined COMSOL option *Electric Currents* was used. See chapter 3.1 for the equations and boundary conditions.

Table 4.1: Material values of electrical conductivity σ and relative permittivity of the specific materials with assigned domains.

Material name	**Domain**	**Electrical conductivity σ in [S/m]**	**Relative permittivity**
Perilmyph	Scala tympani, scala vestibuli	1.43	450
Endolymph	Scala media	1.67	314
Bone	Outer cochlear bone, surrounding tissue	0.016	1307
Bone-Nerve	Modiolus	0.0334	1280
Electrode	Electrodes	1000	1

One of the possible active electrodes was chosen to be the stimulating one and the voltage on it's surface was set to 1 V. Furthermore the grounding was specified at the outer surface of the surrounding box. Note, that since quasi-static conditions are assumed, it is easy to adapt the results of this model to a model with a stimulating voltage of y V. So the results just have to be multiplied with this factor y, see [Rattay et al., 2001b].

The meshing was performed in COMSOL with the predefined element size *fine*. The elements were free tetrahedrons. Fig. 4.3 shows the overall mesh of the geometry and the mesh of the cochlea in more detail.

The study was a stationary computation of the electric potential. A discussion why this is justifiable, was given in chapter 3.1. Fig. 4.4 shows the electric potential for a cut through the xz- and the yz-plane at the height of a defined active electrode at the mid of the cochlea. For every electrode the study was repeated.

4.4 Current on the electrode surface

All the studies were performed with a voltage of 1 V on the surface of the stimulating electrode. However, it also was necessary to find out the current on the electrode surface. This was performed the following way: after solving the model, the current density norm on the electrode surface was integrated in COMSOL. Doing this for all the apical electrodes (except for the most apical with the reduced radius), the value ranged between 0.19 and 0.25 mA. Theoretically the value should be the same for all electrodes. However, the FEM is not an exact method for solving differential equations and the result also depends on the quality of the mesh. This explains the deviation.

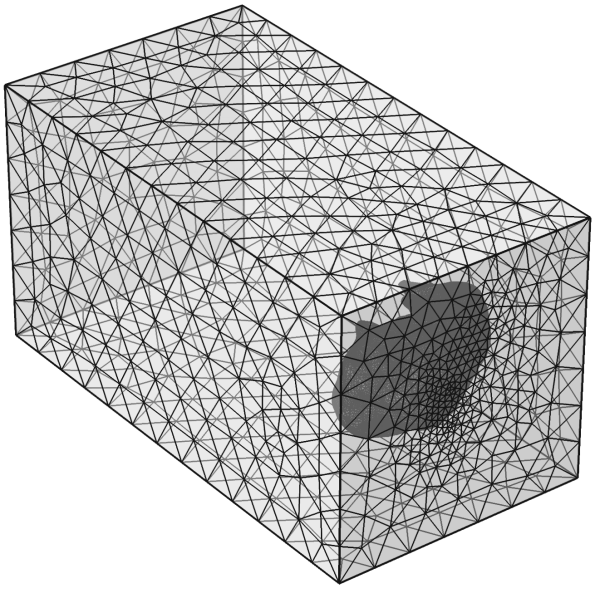

(a) Complete mesh.

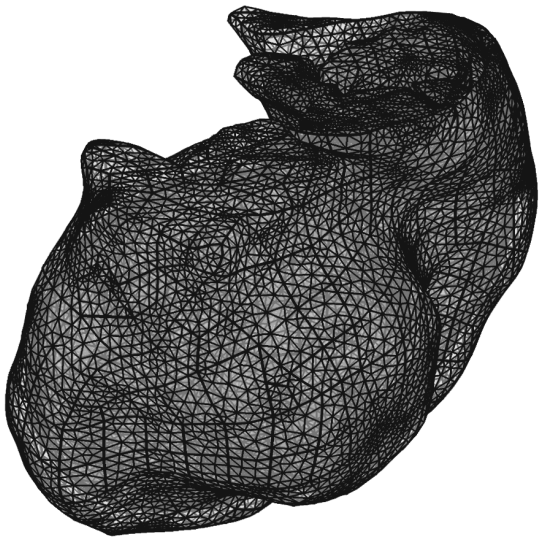

(b) Mesh of the cochlea only.

Figure 4.3: Mesh of the geometry.

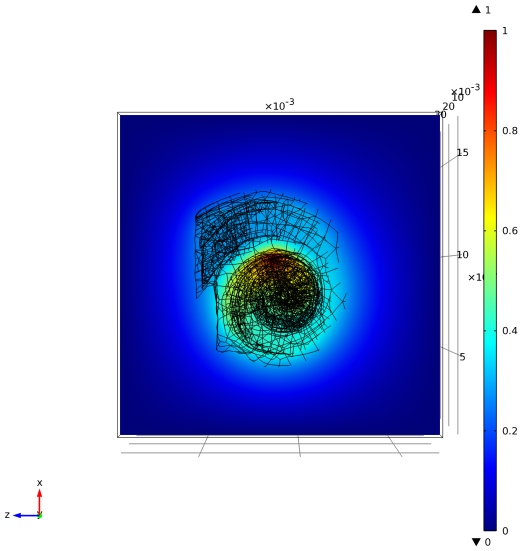

(a) Top view in y direction.

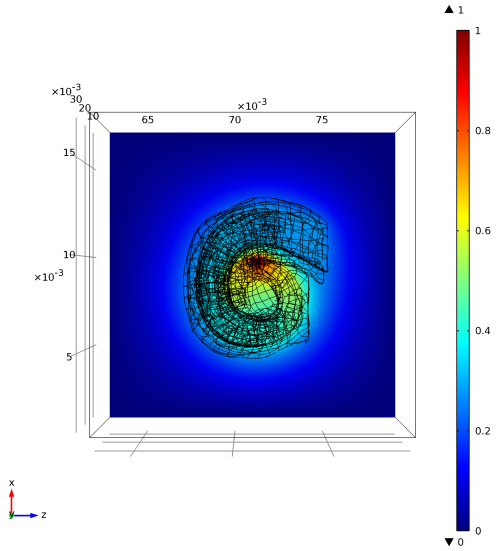

(b) Down view in y direction.

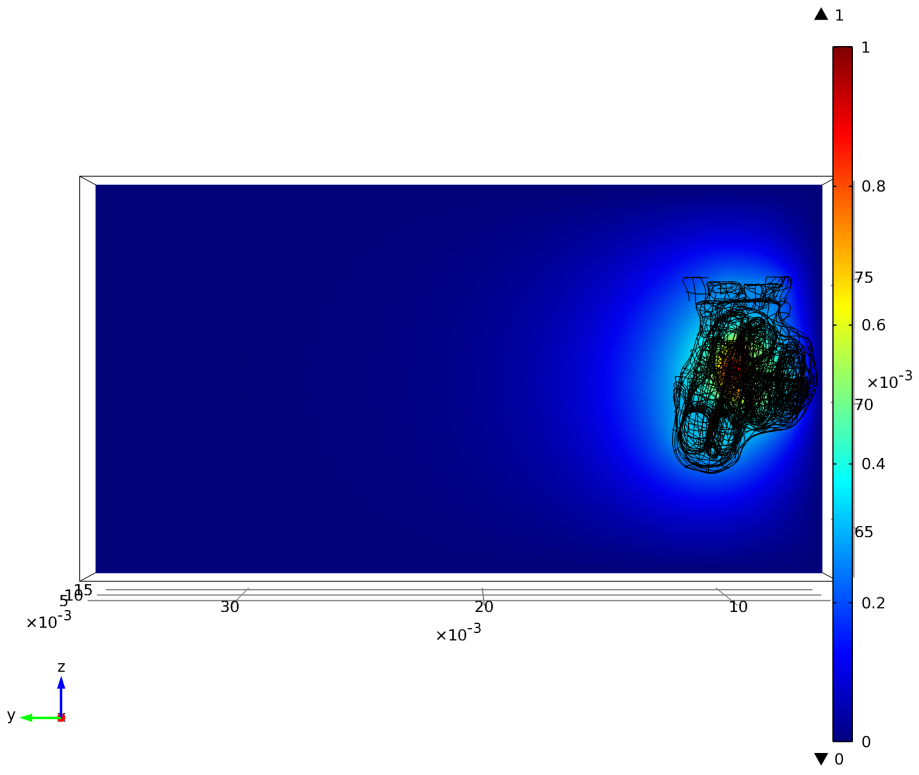

(c) View in x direction.

Figure 4.4: Potential distribution in the geometry for an example electrode in the mid of the cochlea.

Since the range is not too big, the discrepancy is justifiable. As standard value of the current for a voltage of 1 V on the electrode surface, the value 0.215 mA was chosen for further calculations.

Chapter 5

Implementation in Matlab

After the description in chapter 4, how the potential distribution can be obtained in COMSOL, now the modeling of the neural response is explained.

The realistic pathway of thirty fibers was given. These were transformed into a chain of compartments. Now, after defining an stimulus, the differential equations 3.11 to 3.13 were solved. All this was performed with MATLAB R2010a[1].

Cornelia Wenger provided a MATLAB program, which interpolated the fibers, computed the electric potential analytically and solved eq. 3.11 to 3.13, see [Wenger, 2012]. It was partially adapted for this thesis. So a variable dendrite internode length was implemented and the potential distribution calculated in COMSOL was taken into account.

In the following, first of all the modeling of the neurons is presented. Afterwards the parameters of the model are given. Finally the stimulation of the neurons is explained by clarifying the COMSOL-MATLAB interface and the various stimulation modes.

5.1 Modelling of the neurons

In addition to the geometry presented in chapter 4, also several neuron fibers were traced on the images generated by the μCT by T. Potrusil. Finally thirty neuron fibers were provided; they were seven apical, nine mid and 14 basal fibers. Fig. 5.1 presents a illustration of them in the cochlea. Furthermore the soma positions of the fibers were given.

The fibers are denoted as api1 to api7, mid1 to mid9 and bas1 to bas14 beginning in the apex up to the base of the cochlea. They were originally given by data points laying

[1]Registered trademark of The MathWork, Inc.

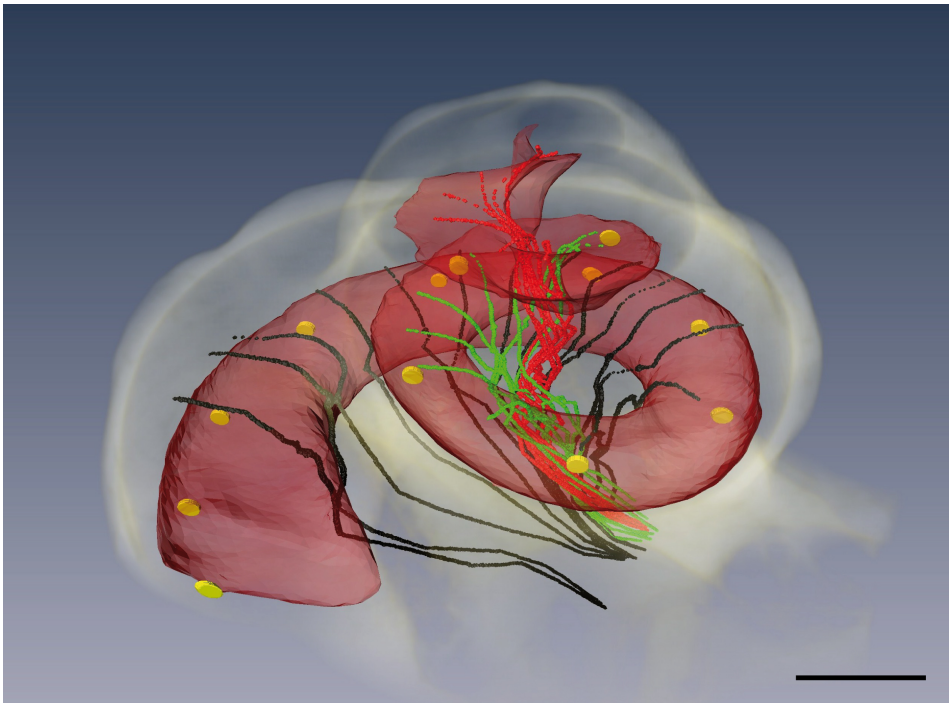

Figure 5.1: Drawing of the traced apical (red), mid (green) and basal (black) neurons in the cochlea. The yellow circles denote electrodes, which are obsolete for this thesis. Image provided by T. Potrusil.

closely together. However, the compartment model described in chapter 3.2 needs fibers as input, which consist of compartments (like soma, nodes, internodes etc.). So the given fibers had to be adapted and converted into a chain of compartments, whereas the natural pathway should be retained. Therefore, on the basis of the information about the position of the soma and compartment lengths, the midpoints of the compartments were interpolated. Furthermore, it was necessary to extend the fibers. The procedure of the interpolation and the elongation is described in more detail in the following.

All neurons are bipolar, which means they have only two processes: one axon and one dendrite. For all fibers the length of the peripheral process and consequently the soma position is given. Furthermore, length parameters for the various compartments are provided.

Generally a neuron is assumed to consist of consecutive compartments as shown in fig. 5.2: at first we have the terminal region of the dendrite, then alternately in a row dendritic internodes and nodes. It is followed by a presomatic compartment, the soma and a postsomatic compartment. Then axonal internodes and nodes alternate in a row; finally a terminal axonal compartment is assumed. The default length parameters are also given in fig. 5.2.

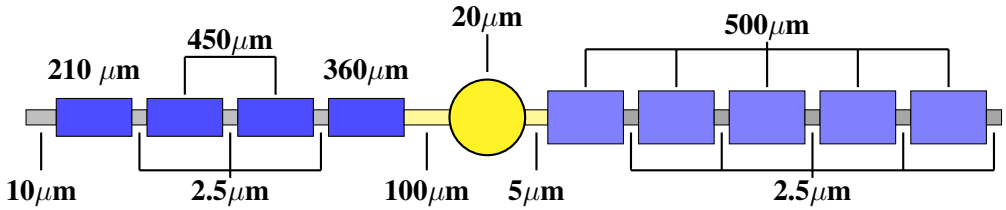

Figure 5.2: Schematic drawing of a neuron with displayed compartment length. On the left side is the dendrite, on the right site the axon. The yellow part is the soma region. Blue boxes denote internodes, grey boxes nodes. Note that this illustration is not to scale. Adapted from [Wenger, 2012].

Based on these informations, the compartment midpoints were interpolated relating to the original pathway. To make sure to fulfill the given length of the peripheral process, the length of the dendritic internodes with a default value of 450μm was adapted if needed. Note, that the exact number of the nodes of Ranvier and internodes of dendrite and axon depends upon the specific neuron.

Of course, the new fibers consisting of consecutive compartments deviate slightly from the original pathway. In fig. 5.3 a 2D projection of the new and the old pathway of a part of fiber api4 are confronted. It shows, that the interpolated pathway is much smoother than the original one. However, the difference between both is not too big.

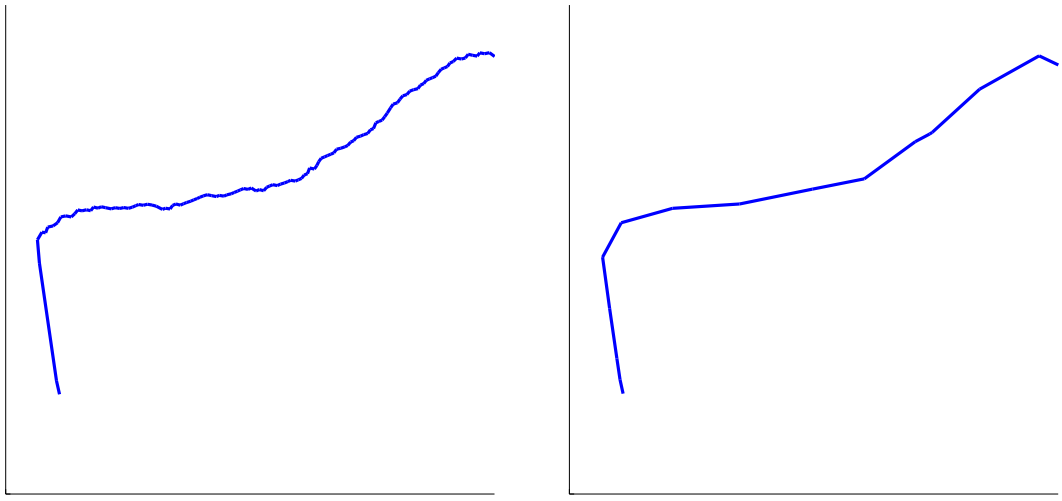

(a) original data (b) interpolated data

Figure 5.3: Confrontation of original and interpolated fiber pathway for a part of fiber api4.

Furthermore, the fibers had to be extended artificially for two reasons: first of all, sometimes, especially in anodic stimulation, an AP was released wrongly at the last compartment. Admittedly, this is an unrequested event, which can be avoided by elongating the fibers. Furthermore, it is an interesting information, how long APs need to reach the brain. To make the results for the fibers comparable, all fibers should end in the same plane. The durations of the APs until reaching this endpoint are then comparable for the fibers. The extension of the fibers should not have an effect on the (correct) site of initiation of APs and is therefore feasible.

The extension was performed the following way: the elongation was in the direction of the ends of the specific fibers. A short part of the end of every fiber was taken and interpolated as a line. This line was attached to the end of the corresponding fiber. The fiber bas6 was taken as reference fiber: it was elongated to finally have 61 compartments. Then a plane was built consisting of the (new) endpoint of bas6 and having the direction vector of it's interpolated line as normal vector. The remaining fibers were elongated up to this plane.

Furthermore, there was the option to assume the neurons to be degenerated, which means the peripheral dendrite is missing. In this configuration, the neurons start right from the soma.

5.2 Parameters of the model

The parameter values like compartment diameters or conductances base in principle on the default values given in [Wenger, 2012], which generally follow [Rattay et al., 2001a].

The default length and diameter values of the compartments are presented in figure 5.2. Note that the default length of dendrite internodes (INs) except for the first and last one is set to 450μm. However, as noted above, to fulfill the given length of the peripheral process, the concrete value is adapted. For most fibers the length is between about 123% and 80 % of the original value. However, for mid5 and mid9 the value is almost 150%, since their dendrites only have three internodes. Luckily the IN length (except for the last one before the soma) has negligible effect on initiation site or AP duration, see also section 7.2. This means this adaptation is feasible.

Table 5.1 lists the compartment depending parameter values of the length x, diameter d, number of myelin layers n_{myel} and the constants of maximum conductance per cm^2 of sodium, potassium and leakage g_{NaHH}, g_{KHH} and g_{LHH}.

The dendrite diameter d is set to 1.3 μm, whereas the axonal dendrite is twice as high and 2.6 μm. [Potrusil et al., 2012] presents average soma diameters for apical, mid and basal fibers as $d_{api} = 20.1$ μm, $d_{mid} = 18.79\mu$m and $d_{bas} = 18.86$ μm; however, here as standard diameter $d_{standard} = 20$ μm is taken for all fibers.

The number of myelin layers n_{myel} depends on the compartment type: it is one for

Table 5.1: Compartment depending parameter values of the Hodgkin-Huxley compartment model; compartment length x, diameter d, number of myelin layers n_{myel} and constants for maximum conductance per cm^2 g_{NaHH}, g_{KHH} and g_{LHH} in mS/cm^2 are given.

	Compartment name	x	d	n_{myel}	g_{NaHH}	g_{KHH}	g_{LHH}
Dendrite:	terminal of the dendrite	10μm	1.3μm	1	1200	360	3
	dendritic internode	210 to 675μm	1.3μm	40	0	0	1
	dendritic node	2.5μm	1.3μm	1	1200	360	3
Soma:	presomatic compartment	100μm	1.3μm	3	1200	360	3
	soma	20μm	20μm	3	120	36	0.3
	postsomatic compartment	5μm	2.6μm	3	1200	360	3
Axon:	axonal internode	500μm	2.6μm	80	0	0	1
	axonal node	2.5μm	2.6μm	1	1200	360	3
	terminal of the axon	2.5μm	2.6μm	1	1200	360	3

the terminal regions and the nodes. The somatic region consisting of pre- and postsomatic compartment and the soma itself are assumed to have three myelin layers. However, the number of myelin layers of internodes is 40 for dendritic and 80 for axonal internodes.

Note, that the internodes are passive compartments and therefore no sodium and potassium current is assumed; hence we have $g_{NaHH} = 0$ mS/cm^2 and $g_{KHH} = 0$ mS/cm^2, whereas for the leakage current we have $g_{LHH} = 1$ mS/cm^2. For active compartments like the terminal and the pre- and postsomatic compartments and nodes we have values of $g_{NaHH} = 1200$ mS/cm^2, $g_{KHH} = 360$ mS/cm^2 and $g_{LHH} = 3$ mS/cm^2. For the soma, the values are reduced to a tenth and they are $g_{NaHH} = 120$ mS/cm^2, $g_{KHH} = 36$ mS/cm^2 and $g_{LHH} = 0.3$ mS/cm^2. Note that, as noted in chapter 3.2, the concrete value of the leakage maximum conductance is inversely proportional to the number of myelin layers and hence $g_L = g_{LHH}/n_{myel}$.

Table 5.2: Parameter values of intracellular resistivity, membrane capacitance, temperature coefficient, resting potential and battery voltages of sodium and potassium.

Parameter	**Symbol**	**Value**
Intracellular resistivity	ρ_i	0.05 kΩcm
Membrane capacitance	c	1 μF/cm^2
Temperature coefficient	k	12
Resting potential	V_{rest}	-70 mV
Sodium battery voltage	V_{Na}	115 mV
Potassium battery voltage	V_K	-12 mV

Further parameters of the model are listed in table 5.2. The intracellular resistivity was set to $\rho_i = 0.05$ kΩcm, the membrane capacitance to $c = 1$ μF/cm^2 and the temperature coefficient k was set to 12. The battery voltages V_{Na}, V_K and V_{leak} were the following: for potassium and sodium $V_{Na} = 115$ mV and $V_K = -12$ mV are stated. However, the leakage battery voltage is more complicated. It is set to

$$V_{leak} = -V_0 + (I_{Na}(0) + I_K(0))/g_L, \tag{5.1}$$

with

$$I_{Na}(0) = g_{Na} m(0)^3 h(0)(V_0 - V_{Na}), \tag{5.2}$$

$$I_K(0) = g_K n(0)^4 (V_0 - V_K) \tag{5.3}$$

and $V_0 = 0$. For $m(0)$, $n(0)$ and $h(0)$ see equations 3.16a to 3.16c.

5.3 Modelling of the stimulation of the neurons

The fibers were implemented in the MATLAB model as described above. How the stimulation was modeled, is described in this section. Natural hearing can be modeled by an intracellular stimulation at the first compartment. However, the fibers also can be stimulated extracellularly by the electrodes. Then the potential field generated by the electrodes stimulates the neurons. This field was computed in COMSOL as described in chapter 4. How this data can be imported into MATLAB is described in the following. Afterwards the various stimulation types are explained.

Comsol - Matlab - Interface

The COMSOL results had to be imported into MATLAB; one needed the potential value at the compartment midpoints. This was done by interpolating the value of the potential computed in COMSOL for a specific electrode at the compartment midpoints of the fibers.

There is the option to control COMSOL via MATLAB by the program LiveLink™ for MATLAB. It allows to work with the MATLAB desktop and so one has the possibility of using all the MATLAB functions; but there are also further functions to be able to work with COMSOL files. Via the command

```
model=mphload('modelname.mph');
```

a COMSOL model can be imported to MATLAB. Afterwards the voltage V at the compartment midpoints (x, y, z) can be obtained by the command

```
V_stim=mphinterp(model,'V','coord',[x';y';z'])';
```

As noted above, quasi-static conditions are assumed. Therefore the results can easily be adapted for assuming a stimulating electrode of y V, by multiplying the values at every compartment midpoint by the factor y.

Stimulation modes

Like in [Wenger, 2012], there are generally four stimulation types: an anodic and a cathodic monophasic pulse, abbreviated by ANO and CAT. Furthermore a biphasic stimulation is possible: these pulses are either an anodic pulse followed by cathodic pulse (BIA) or first a cathodic, then an anodic pulse (BIC).

The duration of the monophasic pulses is 100 μs, in biphasic stimulation the pulse length is 100 μs for each phase, this means altogether a stimulation length of 200 μs. The stimulation amplitudes depend on the specific computations.

Chapter 6

Analysis of the model

The model consisting of a COMSOL and a MATLAB part was presented in chapter 4 and 5. Now it is necessary to check, whether the computed results are reasonable, on which parameters they react sensitively and how electrodes and the excitability of neurons correspond. Therefore this chapter is divided into a section about the validation of the model and a section about how distance, external voltage V_e and excitability of the fibers are connected.

6.1 Validation of the model

For the validation, first of all it is investigated, whether the computed external potential V_e is reasonable. Furthermore the material values are of course not exact. Therefore the sensitivity of the model towards changing the electrical conductivity was evaluated. Actually, the concrete geometry of the COMSOL model was quite arbitrary. This means the size of the box and the configuration of the grounding also could be different. Therefore it would be necessary to check it's influences, but this was not evaluated structurally in this thesis due to the too high effort.

Check of the potential along an example fiber

When validating the model, it is necessary to check, whether the external potential V_e along the fibers is reasonable. This is done here for the fiber mid2 for the electrode EL10 at $630°$ as representatives. It is also checked, what influence the interpolation of the fiber (see chapter 5) can have on V_e.

Fig. 6.1 shows the different materials through which the original and the interpolated fiber mid2 are passing as well as the external potential of V_e for EL10 along the length.

Actually, the course of the fibers through the different materials is unexpected: one would assume the fiber to go first through the scala media and to enter then the modiolus, before ending in the outer box. However, fig. 6.1 shows, that the fiber is going through a bony compartment at first, then through an endolymph filled cavity and afterwards again through a bony compartment. Finally the fiber is going through the modiolus and then it reaches the outer bony box. This holds for the original as well as the interpolated fiber. The reasons for the unexpected pathway are various: first of all the limited resolution and the small distance of the fibers towards the different geometric components, as well as various complicated intermediate steps when creating the geometry of the cochlea and the pathway of the fibers caused the special pathway. Therefore most of the other fibers have a similar unexpected pathway, however the exact course differs. For the example fiber mid2, the interpolation has negligible influence on the materials along the fiber. However, theoretically also the interpolation could cause some deviations from the assumed pathway.

After the description of the course through the geometric components, a comparison of V_e along the original and the interpolated fiber mid2 for EL10 is given. As displayed in fig. 6.1, some of the fine structure of V_e in the peripheral process is lost in the interpolated fiber in comparison to the original fiber. The difference is not too big, since the main structure of V_e of the original data also holds for the interpolated fiber. However, there is a noticeable difference in the local minimum of the fibers at about $x = 0.025$ cm, which is $V_{\text{locmin,original}} = 0.630$ V respectively $V_{\text{locmin,interp}} = 0.656$ V. For the normal fibers the stimulation is mainly in the peripheral process. Hence the deviations could have big consequences, when thinking of the possibility of loosing even a small peak due to the interpolation of the fiber's pathway.

When comparing the course of V_e and the conductivity values σ along the fiber, some of the sharp bends of V_e can be explained. For example the bend at $x = 0.35$ cm can be explained by the crossover of the fiber from the modiolus to the outer box. However, the sharp bend at the local minimum at about $x = 0.025$ cm does not coincide with a change in the material. The unexpected short run of the fiber through an endolymph-filled cavity seems to have negligible consequences.

It is possible to compare the course of V_e to results from [Rattay et al., 2001b]. The cochlear geometry of this older model is simplified. However, it is also solved by the FEM and has a similar configuration and material values like the model described in this thesis. The range of V_e, better visible in fig. 6.2, is comparable to the one of [Rattay et al., 2001b]. However, the course of V_e is not as smooth as in the old model.

In conclusion, the partially unwanted pathway of the fibers through geometric parts of the model, could be avoided only with high effort, but has partially consequences on V_e. The interpolation could have negative effects, when thinking about loosing small peaks. However, avoiding this would also be combined with a lot of work. The un-

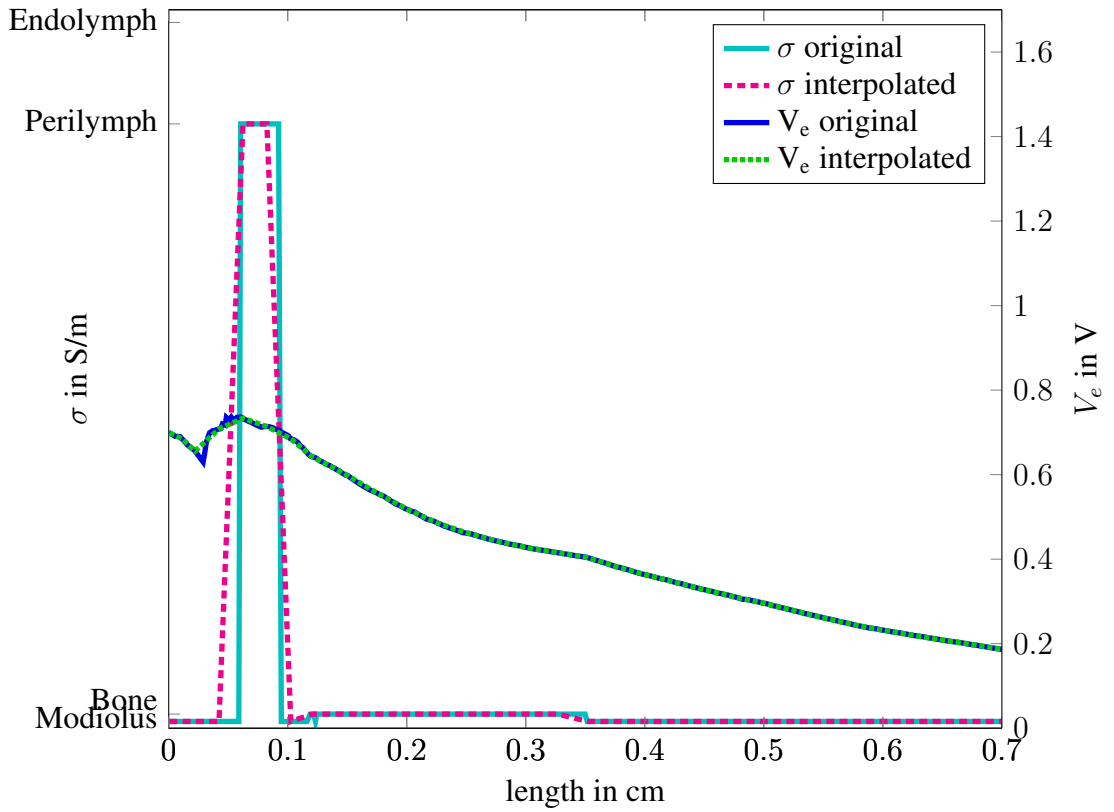

Figure 6.1: Comparison of electrical conductivity σ and external potential V_e along mid2 for the original and the interpolated course; the voltage is given in V for 1 V at the electrode surface of EL10.

smoothness of V_e is partially worrying, since it is not necessarily realistic. However, the range of V_e seems realistic. But even when it is not absolutely correct, this rather has an effect on the size of the THs. So the THs should be interpreted as rather quantitative than qualitative results.

Sensitivity of the model towards material values

Like in [Rattay et al., 2001b], it was evaluated what consequences changing the electrical conductivities has on the external voltage V_e along a neuron. Thus the electrical conductivities of the materials bone and bone-nerve were double and halved; the conductivity values of the fluids endolymph and perilymph were only set to the doubled value. The comparison of V_e along mid2 for EL10 for the various material configurations is given in fig. 6.2.

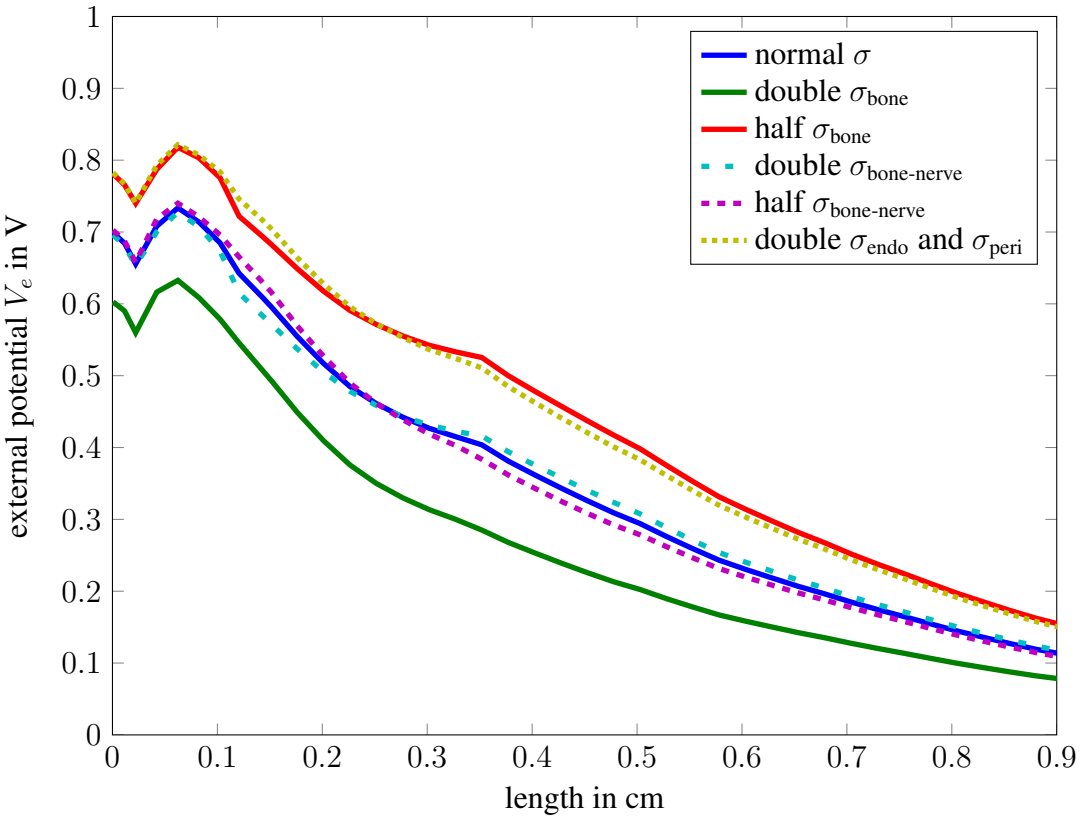

Figure 6.2: Comparison of external potential V_e in V along mid2 for various changes of the electrical conductivity σ for 1 V at the electrode surface of EL10.

It is remarkable, that the shape of V_e is similar in all cases. However, at $x = 0.35$ cm the curves for doubled σ_{bone} and halved $\sigma_{\text{bone-nerve}}$ are much smoother than the other ones. This comes from the fact, that in both configurations the conductivities of bone and bone-nerve are very similar ($2 \cdot \sigma_{t\text{bone}} = 0.032 S/m$ and $\sigma_{\text{bone-nerve}} = 0.0334 S/m$ respectively $\sigma_{\text{bone}} = 0.016 S/m$ and $0.5 \cdot \sigma_{\text{bone-nerve}} = 0.0167 S/m$. Therefore then the course from the modiolus to the outer box has only marginal consequences. Furthermore changing the bone's and fluids electrical conductivities results in a shift respective to the normal material values: halving the bony and doubling the fluid's conductivities leads to a higher potential, whereas doubling σ_{bone} causes a lower potential. However, the distance towards the original V_e gets smaller when reaching the end of the fiber (so when the fiber enters the bone compartment and the influence of the grounding becomes higher). Changing the electrical conductivity σ of the bone-nerve material does not have considerable consequences on V_e in comparison to the default, normal configuration.

When comparing the threshold (TH) and initiation site (IS) of an action potential of mid2 for EL10 for the different material configurations of fig. 6.2, it turns out, that

changing σ does not have much impact. THs and ISs are listed in table 6.1. The THs are all comparable and the ISs stay the same in most cases. Exceptions are the ISs for the CAT stimulus, which are either at the first, the fifth or the ninth compartment and for the BIA stimulus, whose ISs are either at compartment one of five.

These results show, that the model is not too sensitive regarding a change of the material values in most cases, but the ISs might change.

Table 6.1: Thresholds in mA and initiation sites of fiber mid2 for EL10 for the various tests of changing the values of the electrical conductivity.

	CAT		**ANO**		**BIC**		**BIA**	
Material test	TH	IS	TH	IS	TH	IS	TH	IS
Normal	0.065	1	0.09	1	0.06	1	0.085	5
Double bone	0.075	5	0.09	1	0.06	1	0.085	1
Half bone	0.065	1	0.095	1	0.065	1	0.085	5
Double bone-nerve	0.06	1	0.1	1	0.06	1	0.085	5
Half bone-nerve	0.07	9	0.08	1	0.06	1	0.08	1
Double fluids	0.075	5	0.085	1	0.065	1	0.085	5

6.2 Relationship between electrode-to-fiber-distance, external potential V_e and excitability

This section explains the relationship between the fibers and the electrodes. First of all, the distance between electrodes and fibers is given. It is followed by assumptions about the relationship between the distance between electrode and fiber and the external potential V_e along the fibers. Afterwards the excitability of the fibers is mentioned

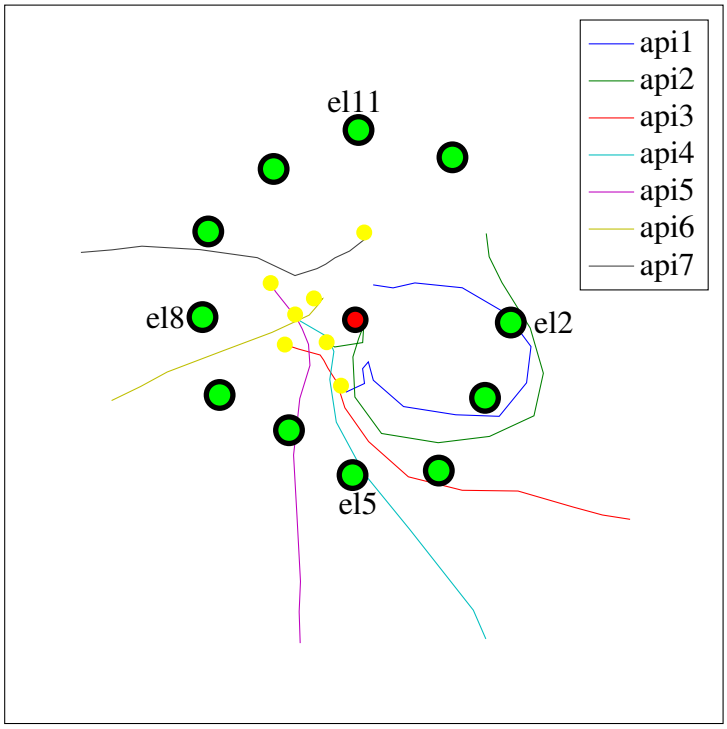

Figure 6.3: Top view regarding to the midmodiolar axis (red circle) on the peripheral processes of the apical fibers and the apical electrodes (green circles). The somata are given by yellow circles.

Distance from electrode to fiber

First of all the geometric relationship between the fibers and electrodes is investigated. This is done by evaluating the distance between both.

Fig. 6.3 presents a top view respectively to the midmodiolar axis on the peripheral processes of the apical fibers and the electrodes 2 to 12. It gives a rough idea of the distance of the peripheral processes towards the electrodes. It especially shows, that api1 and api2 have a quite low distance towards EL2 to EL6 due to their highly spiraling shape. However - to a smaller extent - also the other fibers seem to approach to several electrodes along their peripheral process - e.g. api3 to EL4 to EL7.

Anyway, fig. 6.3 is only a top view on the fibers and electrodes, and hence does not give any information about the central process and the z coordinate - which means it does not show the real distance. However, instead of investigating for all electrodes the distances towards the fibers, only a selection is presented here. So the distances towards the apical fibers are shown for the three selected electrodes EL2, EL5 and EL10 in fig. 6.4.

These distance plots help to get a first idea, which fibers might are most sensitive to

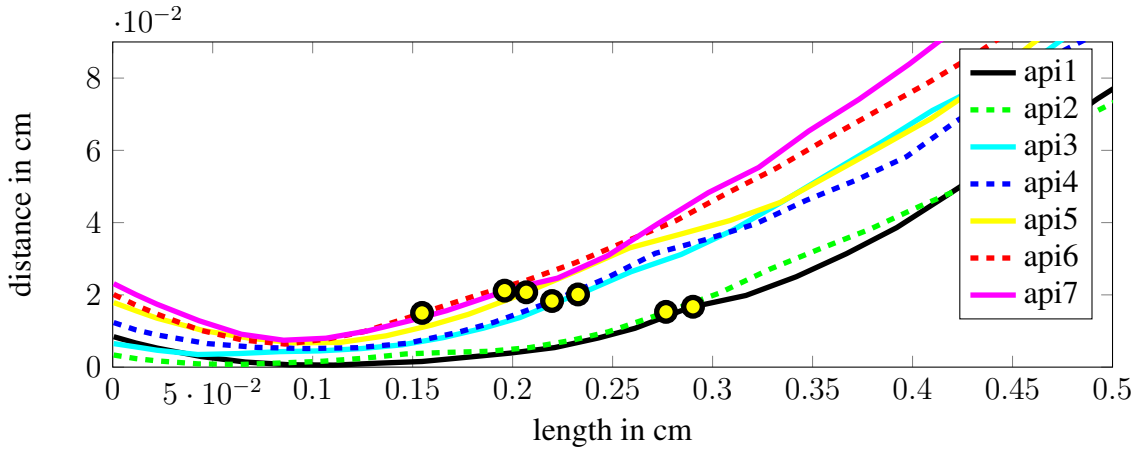

(a) electrode 2

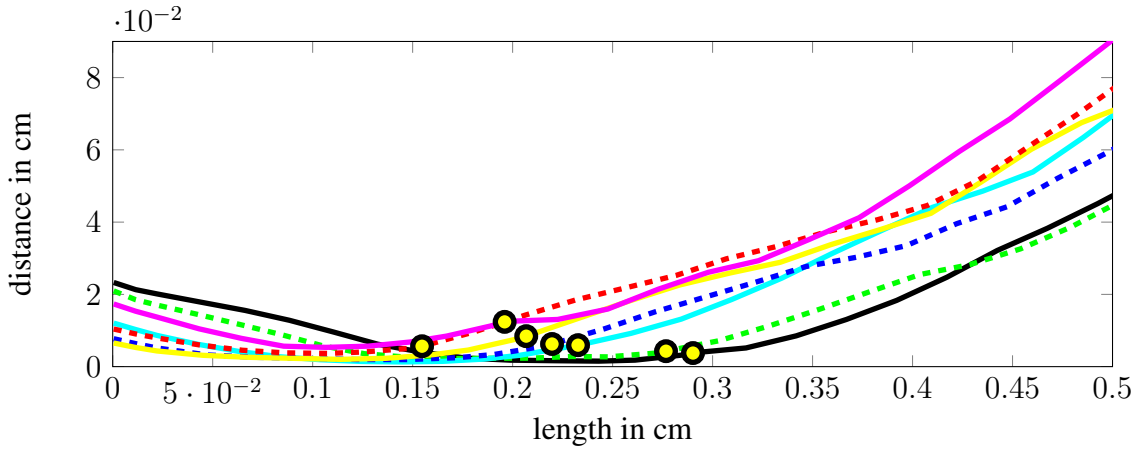

(b) electrode 5

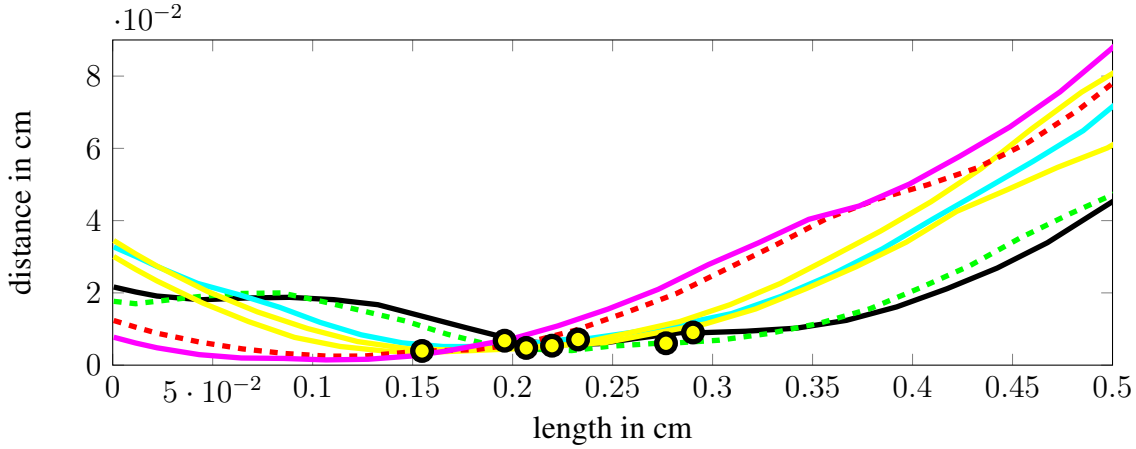

(c) electrode 10

Figure 6.4: Distance along the length of the apical fibers towards the electrodes EL2, EL5 and EL10.

a given electrode. So the very apical electrode 2 in fig. 6.4a has lowest distance to the the most apical fibers api1 and api2. Furthermore api4 and api5 are the nearest fibers for electrode 5 in fig. 6.4b at their peripheral process, whereas api1 and api2 have a comparable distance around their somata and at the central process. The fibers api6 and api7, however, have the smallest distance towards the more middle placed electrode 10 at their peripheral ends, as given in fig. 6.4c. Again both fibers api1 and api2 are the nearest fibers at the soma and their central processes, but the distance is generally higher than for api6 and api7.

This fact, that the most apical fibers api1 and api2 are the nearest towards all the electrodes around their somata and at the central process, is very interesting. It results from the fact, that both fibers spiral a lot and with a greater radius than the other apical fibers. This fact is important, since it can have the result, that they are might not the most sensitive fibers for a certain electrode, but more easily stimulated than some neighboring fibers of the most sensitive one. This means that the tonotopic principle is violated. That this really happens is described later in chapter 8.

However, the next step is to find out, how distance towards an electrode and external potential along the length of a fiber correspond.

Electrode-to-fiber-distance and external potential

At first a view on the electrode-fiber-distance was given above in fig. 6.4. Now the relationship between the distance towards an electrode and the resulting external potential V_e along the neuron length is investigated. So fig. 6.5 presents the external potential V_e along the apical fibers when setting the voltage at the electrode surface to 1 V.

First of all, two peculiarities are eye-catching: clearly smaller distance between electrode and fiber does not necessary correspond with a higher external potential. Furthermore, there are partially sharp bends along V_e. Both observations partially result from the inhomogeneity of the tissue corresponding to the electrical conductivity, see also chapter 6.1.

The different electrical conductivities σ of the geometric components have an effect on the distribution of the electric potential caused by the active electrode and the grounding. For example the electrical conductivity $\sigma_{\text{peri}} = 1.43 S/m$ of the perilymph in the scala tympani is about four times greater than $\sigma_{\text{mod}} = 0.0334 S/m$ of the bony-nervous modiolus. These extensive differences result in a non-linear relationship between the distance towards the electrode and the electric potential V_e. Furthermore it can cause great deviations of V_e in small environments, which then can result in sharp bends along a pathway.

Therefore it is not feasible to consider only the distance towards the electrode for making assumptions about the sensitivity of an fiber towards an electrode. However, sometimes rough speculations are possible, that a nearer fiber also results in a higher potential: for EL2 the nearest fibers api1 and api2 always have the highest V_e; and also

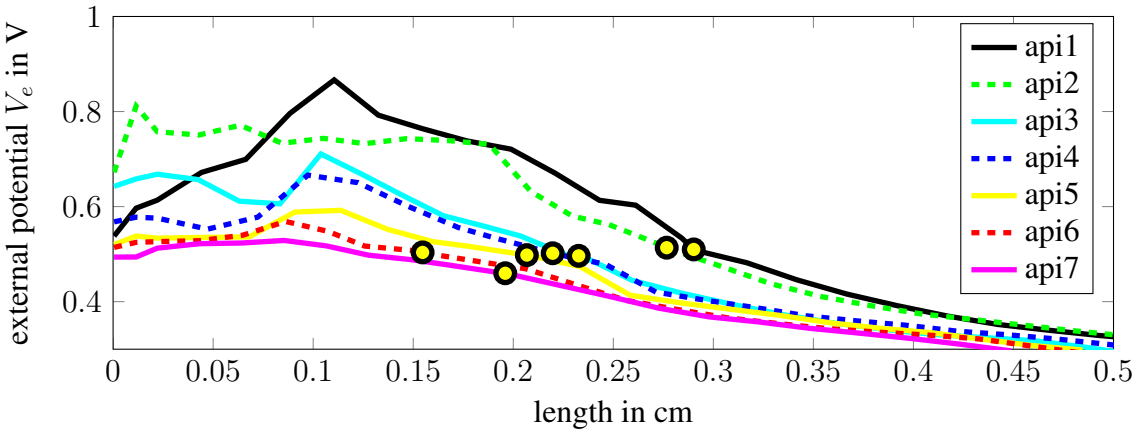

(a) electrode 2

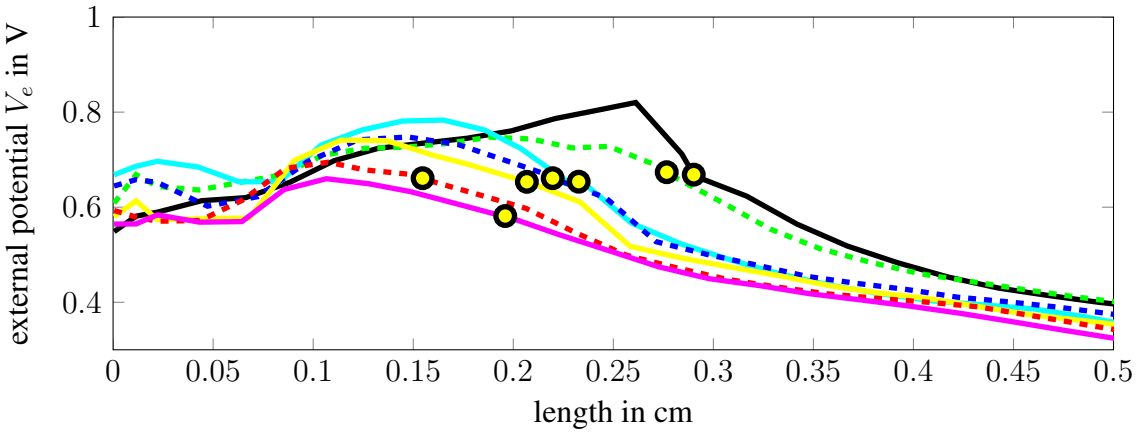

(b) electrode 5

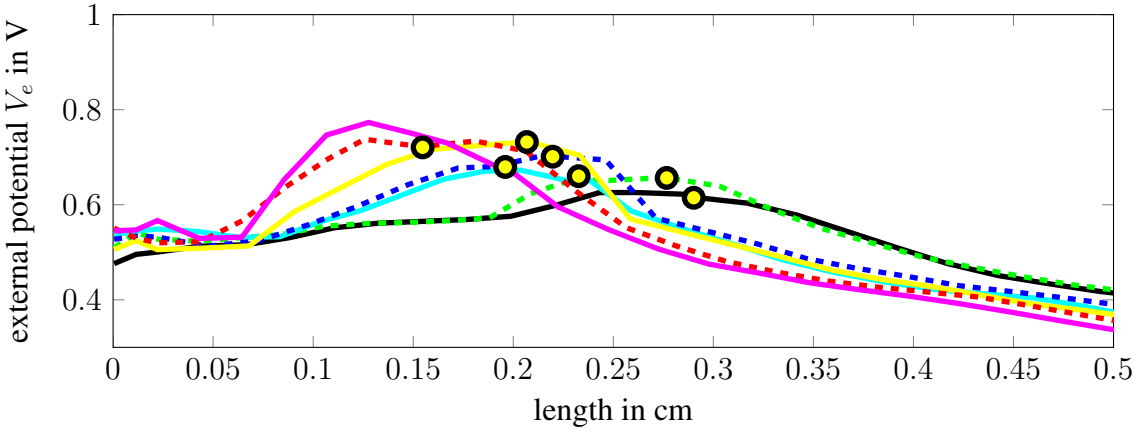

(c) electrode 10

Figure 6.5: External potential in V along the length of the apical fibers for electrodes EL2, EL5 and EL10 for 1 V at the respective active electrode.

for EL10 firstly api6 and api7 have the lowest distance and highest potential; afterwards the same holds for api1 and api2.

The second peculiarity, thus the partially sharp bends of V_e along the fibers, can have big consequences: initiations of APs are possible, which are actually unintended. An example for this is given in chapter 8.2. The reason for this phenomenon is explained in more detail in the following section, which treats the excitability of the fibers and how it corresponds with the external potential. .

External potential and excitability

Of course it is possible to investigate the excitability and the THs and ISs of fibers by solving eq. 3.11 to 3.13 repeatedly. However, this can be quite time-consuming. Another possibility - when exact values are not needed and a rough approximation is adequate - is to check the activating function f or the membrane potential along the fiber for a subthreshold stimulus; this means the electrode's current is too low to elicit an AP, but reactions on the membrane are visible. After explaining the activating function f and the membrane potential, it is demonstrated for an example fiber and electrode, how these functions can be used for making assumptions about the IS. For this also the relationship between the activating function f, the membrane potential, the external potential V_e and the reciprocal distance towards the electrode is elaborated. Finally the membrane potential for api1 to api7 for a CAT and an ANO stimulus for the electrodes EL2, EL5 and EL10 is given.

The activating function f [Rattay, 1998], [Rattay, 1999], is given by

$$f_n = [\frac{V_{e,n-1} - V_{e,n}}{R_{n-1}/2 + R_n/2} + \frac{V_{e,n+1} - V_{e,n}}{R_{n+1}/2 + R_n/2}]/C_n \tag{6.1}$$

for middle compartments and by a reduced form for the first and the last compartment. So it is a part of eq. 3.11. It is a good approximation for what happens in the fiber when the stimulus starts, since it can be interpreted as the slope of the membrane potential at the very beginning. However, the activating function does not take into account the effects of longitudinal or ion currents. When $f > 0$, there is a depolarization at this compartment, when $f < 0$, there is a hyperpolarization. This means, positive peaks of f might coincide with an IS. However, these peaks are not necessarily ISs, especially when the compartment is a neighbor of the soma: this has a high capacity and therefore a lot of current will flow into it. Further information about how to find out ISs with the activating function is given in for example [Rattay et al., 2001a].

Another possibility for predicting the excitability of fibers and possible ISs, is to look at the membrane potential for a subthreshold stimulus. Also here depolarizations are indicators for ISs. Since for the membrane potential eq. 3.11 is solved, also longitudinal and ion currents are assumed. So it allows better predictions than the activating function.

To elaborate the prediction of APs, fiber api5 and electrode EL5 are taken as representatives. In fig. 6.6 the external potential V_e, the curve of the reciprocal distance $1/r$ of the fiber towards the electrode, the membrane potential for a subthreshold CAT respectively ANO subthreshold stimulus with 0.01 mA and the activating function f for this stimulus are given. Note, that the curves are partially compressed and no y-axis values are given for reasons of representation. Furthermore only qualitative values are of interest for this evaluation. The vertical dashed lines denote the soma position (shortly after x=0.2 cm) and possible ISs.

When comparing in fig. 6.6a the four given functions for a subthreshold CAT stimulus, it turns out, that the IS is at the maximum of V_e, of $1/r$ and of the membrane potential. However, it does not coincide with the prominent peaks of f at the beginning of the fiber and after the soma and the activating function has a rather flat peak at the site of initiation. The big peak of f at the beginning is also visible in the membrane potential, however, its height is much lower and no AP is initiated here. This means, that in this example, the membrane potential is better in predicting an IS and the activating function rather suggests misleading IS.

For the ANO stimulus (see fig. 6.6b) there are two possible ISs: for lower current it is at the beginning of the dendrite and when increasing the current it is after the soma. It is eye-catching, that the possible ISs coincide with prominent peaks of f. Only the peak of f at the soma has a greater height. Also the membrane potential has it's peaks at the ISs. This means, that both functions are good indicators for IS. However, here also the membrane potential gives better results, when thinking of the great peak of f at the soma, where no AP is initiated. Interestingly, V_e and $1/r$ don't have their maxima at the ISs; at the IS after the soma both functions even have quite low values. However, at the ISs there are sharp bends of V_e.

Summing up the results, the membrane potential is a much better indicator for ISs than the activating function. For latter a lot of experience is needed. However, the activating function is more easily calculated. In the described case, the external potential allows assumptions about possible ISs only for a CAT stimulus; here the maximum of V_e coincides with the IS. However, for the ANO stimulus the ISs were not at points where V_e has a high value, but at sharp bends of V_e. This shows clearly, that the sharp bends of the external potential can have remarkable consequences, especially for anodic pulses.

Since the membrane potential is a good indicator for ISs, fig. 6.7 and fig. 6.8 show the membrane potential for a CAT and an ANO stimulus of 0.01 mA for the electrodes 2, 5 and 10 for all apical fibers. These figures allow certain statements about the order of stimulation of the fibers and on the IS of the AP.

Concluding from fig. 6.7 and 6.8, for EL2 in both cases api1 to api3 seem to be very sensitive fibers. For EL5 we have api1 and api5, as well as api4 with high reactions on the membrane potential for the CAT and ANO stimulus. For EL10 the three fibers api5 to api7 are possibly stimulated most easily for both monophasic stimulation

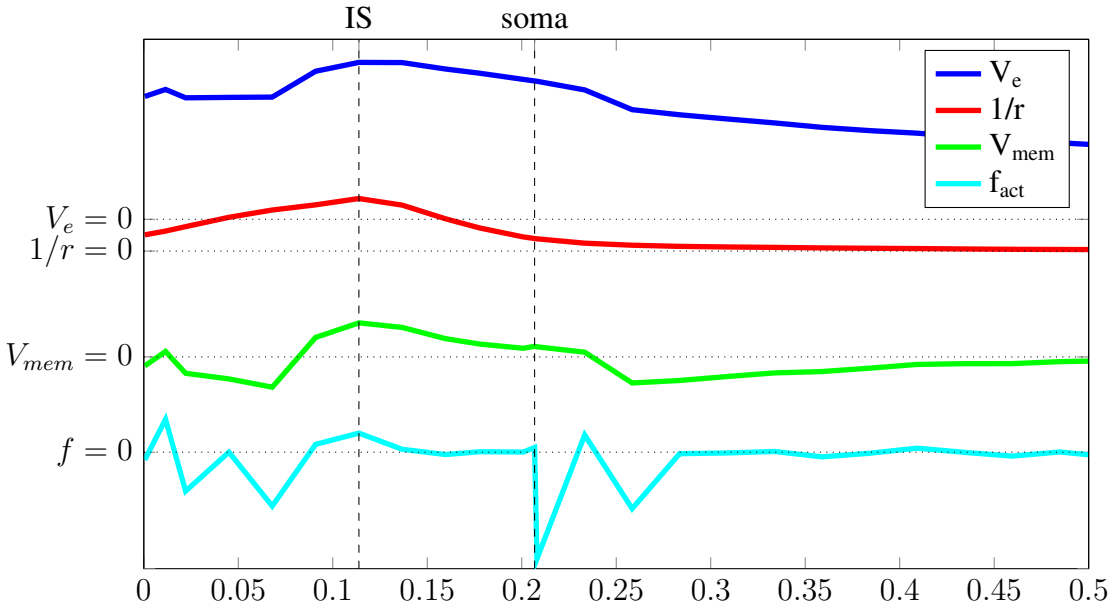

(a) EL5, api5, CAT

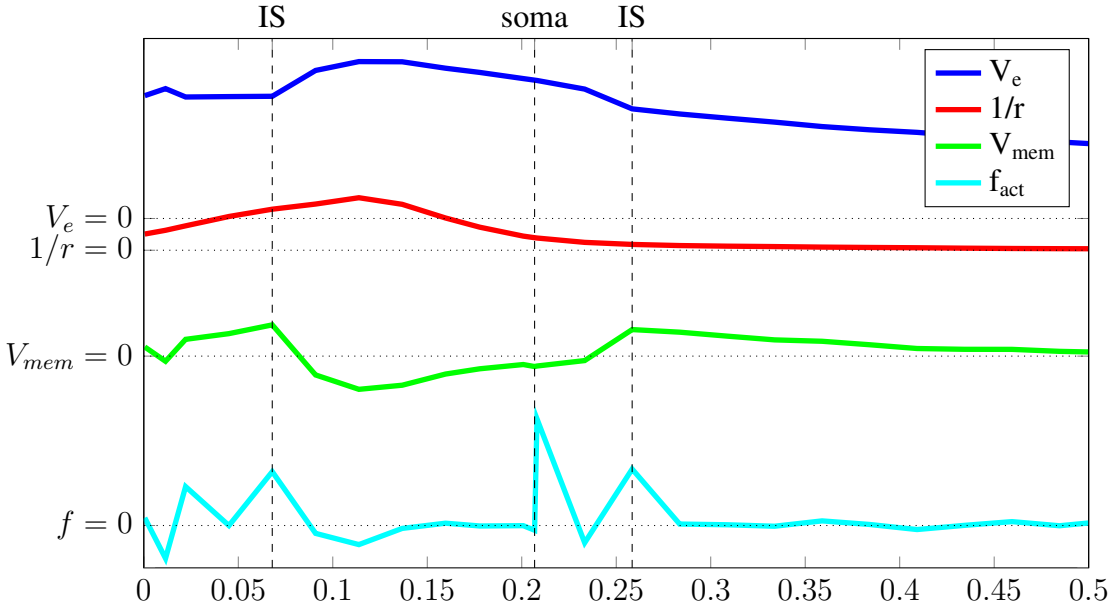

(b) EL5, api5, ANO

Figure 6.6: External potential V_e, reciprocal distance 1/r towards the electrode, membrane voltage and activating function along the fiber length in cm of api5 for cathodic resp. anodic stimulation of EL5. The dashed, vertical lines denote possible ISs and the soma position; the dotted, horizontal lines show where the respective functions are zero. No y-axis is given for reason of representation and since only qualitative values are of interest.

configurations. These assumptions are in accordance with the results of chapter 8.

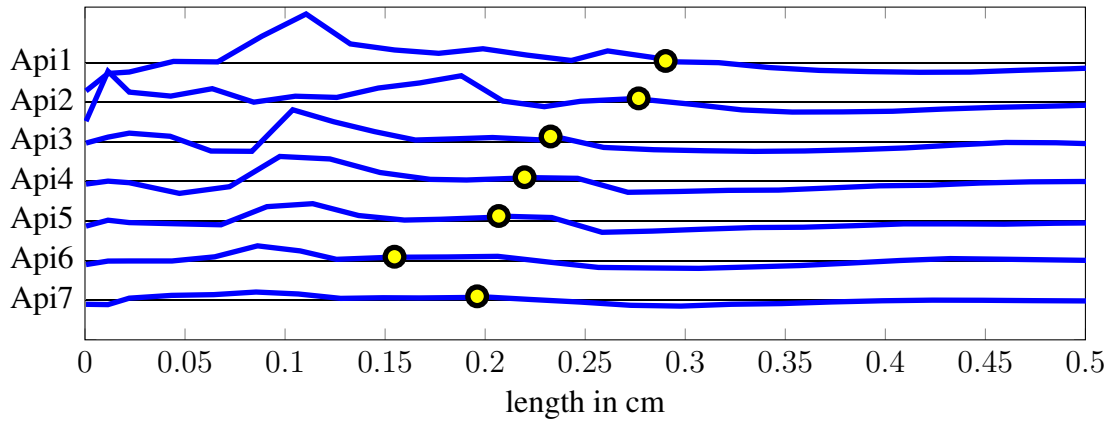

(a) electrode 2, CAT

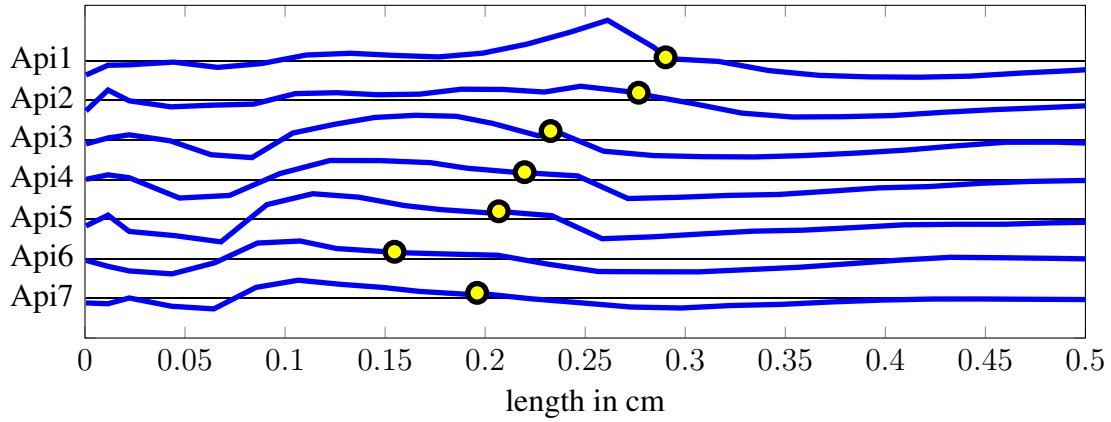

(b) electrode 5

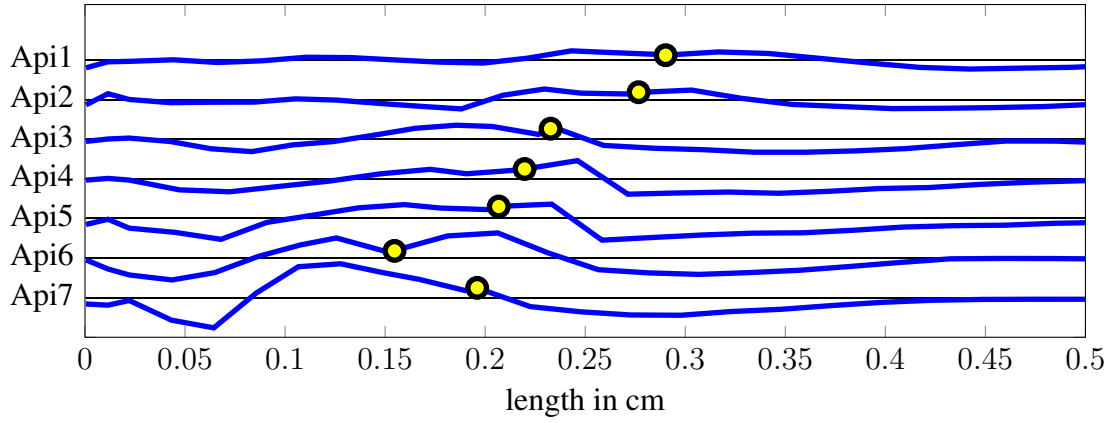

(c) electrode 10

Figure 6.7: Membrane voltage along apical fibers at the end of a subthreshold CAT stimulus. The corresponding black lines denote 0 V. The somata are given by the yellow circles.

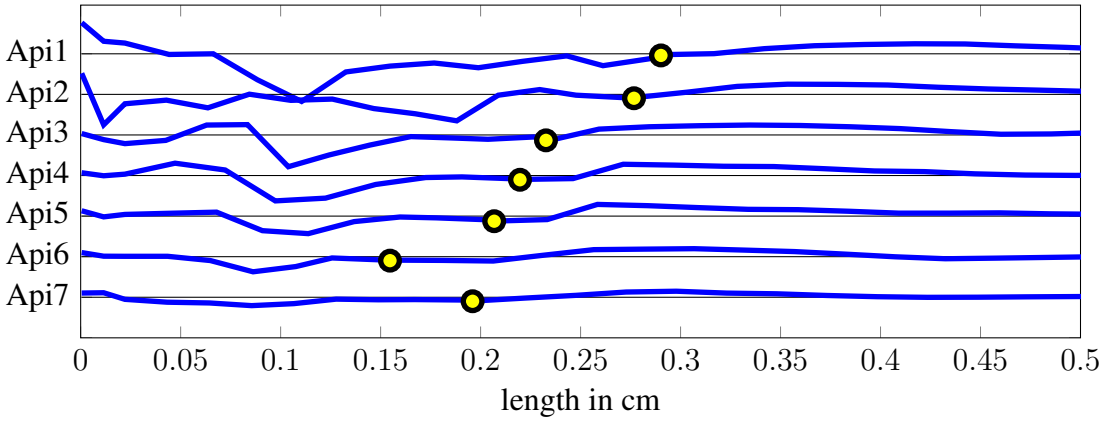

(a) electrode 2, ano

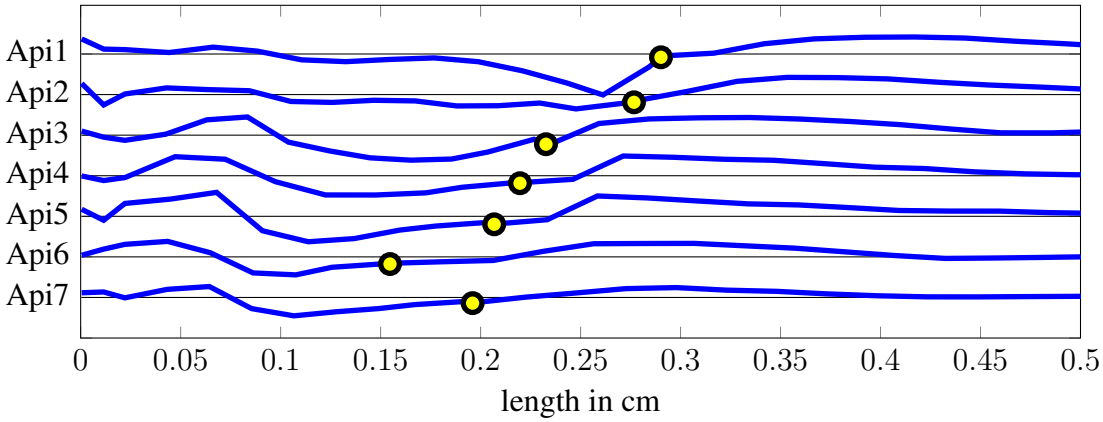

(b) electrode 5

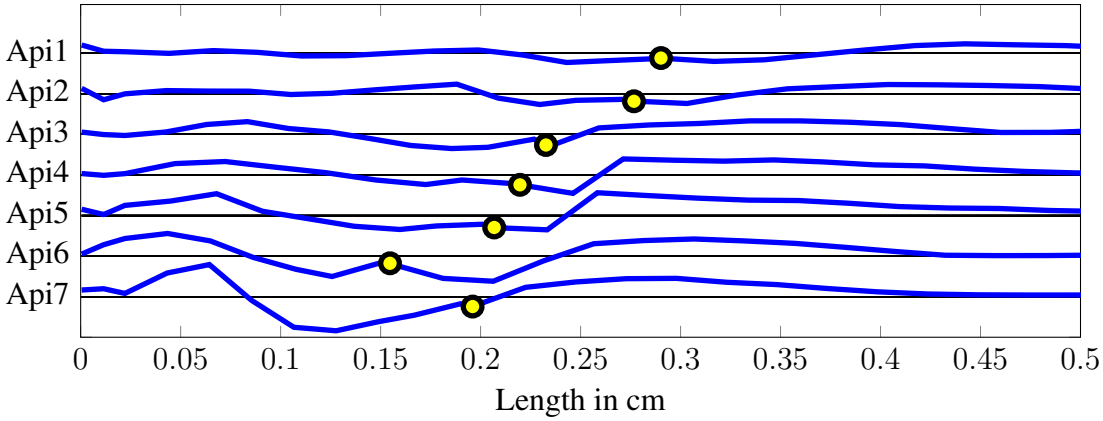

(c) electrode 10

Figure 6.8: Membrane voltage along apical fibers at the end of a subthreshold ano stimulus. The corresponding black lines denote 0 V. The somata are given by the yellow circles.

Chapter 7

Pathway of the fibers and modelling of natural hearing

In this chapter, first of all a comparison of the dendritic length and the pathway of apical, middle and basal fibers is given. Afterwards, the modeling of natural hearing by an intracellular stimulation of the first compartments of the fibers is described.

7.1 Anatomy of the fibers: soma position and pathway

As presented in chapter 5, the realistic pathways of a selection of thirty SGC fibers was given. In this section anatomic peculiarities like the soma position on the fiber and the pathway are described. However, first of all, the realistic fibers are compared to an usual assumption of the pathway of SGCs.

The SGCs are often assumed to be planar and to have a shape like in fig. 7.1. In this figure there is no major difference between apical, middle and basal fibers. However, actually the shape of the fibers is much more irregular. Figure 7.2 shows a representation of the thirty traced realistic fibers of the model.

Extensive differences between the theoretical assumption and the realistic representation are eye-catching: while all the theoretical fibers in fig. 7.1 are planar and smooth, the realistic fibers in fig. 7.2 are irregular, unsmooth and to some extent inordinate. The realistic basal fibers are to some extent more or less planar. However, the realistic apical fibers - and to a lower extent also the middle fibers - have a noticeable partially spiraling shape. Furthermore the length of the peripheral process of the theoretical fibers seems consistent and the same for all fibers. This is not the case for our realistic fibers, as

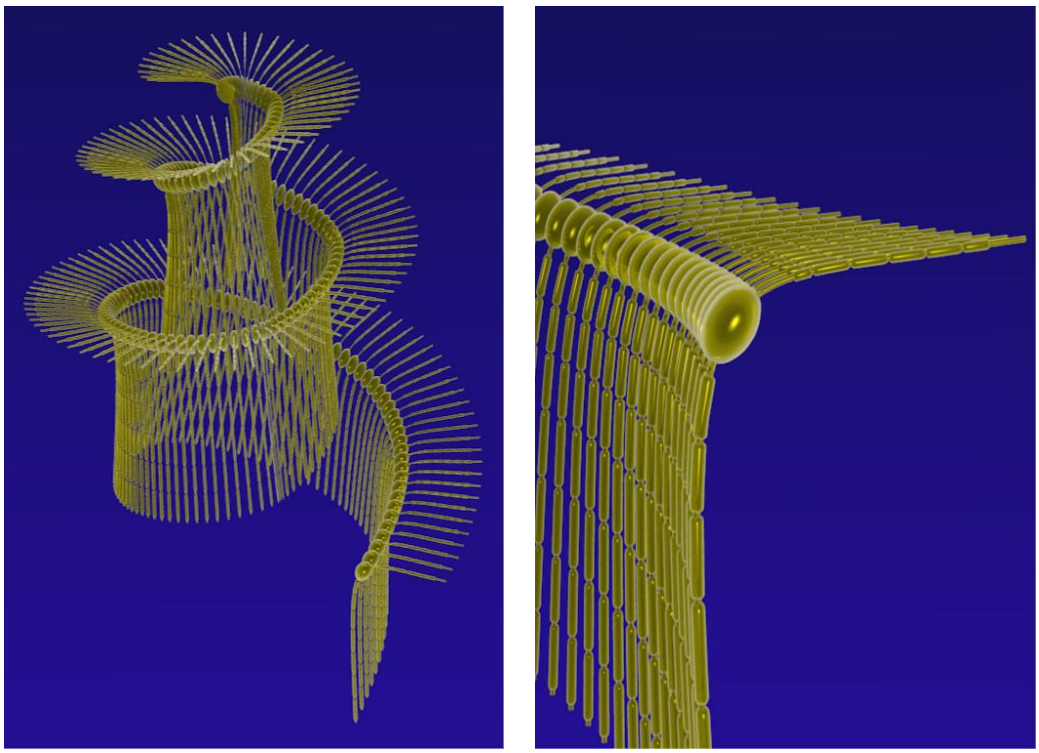

(a) Overall view (b) Detailed view

Figure 7.1: Illustration of theoretical SGCs, taken from [Undurraga, 2013].

presented in more detail later.

All this means, that there is a partially enormous discrepancy between the (theoretical) fibers of fig. 7.1 and the realistic fibers. Therefore it is appropriate to elaborate the geometric pathway of the traced thirty fibers in more detail. First of all, the lengths of the peripheral processes (and so the soma position) of the realistic fibers are investigated. Afterwards the pathways of the fibers are elaborated more extensively.

Soma position

As displayed in fig. 7.3, there are remarkable differences in the peripheral length l_{peri} between the apical, middle and basal fibers, and therefore in the position of the soma on the fiber. So for example the longest peripheral process has api1 with $l_{\text{peri}} = 0.289$ cm, which is about 2.5 times longer than the one of mid8 with $l_{\text{peri}} = 0.123$ cm - the fiber with the shortest measured peripheral process.

Overall l_{peri} is the longest for the apical fibers, decreasing from api1 to api7. The length is highly varying and the apical mean length is 0.224 cm. The middle fibers,

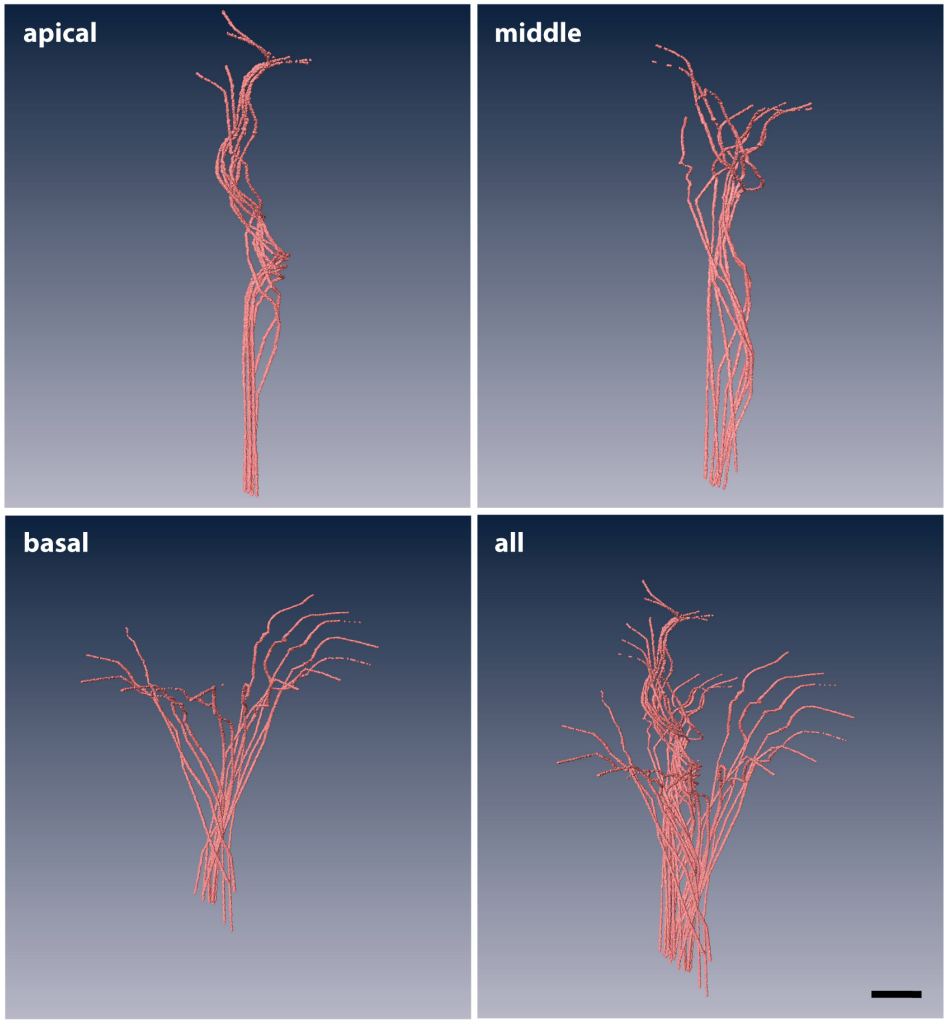

Figure 7.2: Presentation of apical, mid and basal fibers; image provided by T. Potrusil.

however, are the fibers with the overall shortest peripheral process. Their mean length is only 0.144 cm and their length varies only little. Also the length of the basal peripheral processes has a low variance. Their dendrites are generally shorter than the apical ones, but longer than the middle ones. Their mean length is 0.189 cm.

This means, that the assumption of a constant peripheral length for all fibers as in fig. 7.1 is oversimplifying.

Pathway of fibers

The differences in the lengths of the dendrites of the fibers were explained above. This paragraph treats the description of the pathway of the various fibers. First of all, the pe-

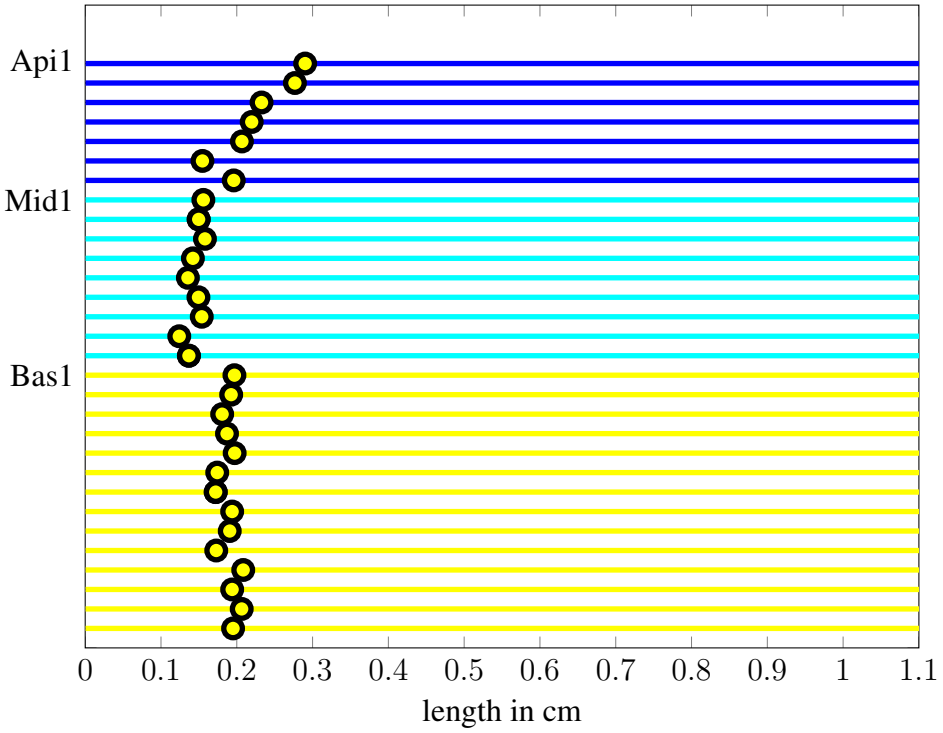

Figure 7.3: Soma position (yellow dots) for the apical (blue), middle (turquoise) and basal (yellow) fibers.

ripheral process is investigated; afterwards the central process and the overall structure are highlighted.

To see the main differences in the pathways of the peripheral processes of the apical, middle and basal fibers in more detail, see fig. 7.4 to 7.7; there separately a 2D top view on dendrites of the apical, middle, basal and all fibers respective to the midmodiolar axis (denoted by a red circle) is shown. The somata are given by yellow circles. Note that these figures show (like the following figures) the already interpolated data (see chapter 5). It is remarkable, that for most fibers the peripheral process looks like a more or less straight line. However, especially the fibers api1 and api2 show a high spiraling. This spiraling of api1 and api2 is also the main reason for their long length of l_{peri} described above.

After this description of the 2-dimensional representation of the peripheral process, the overall pathway is presented. Instead of showing all thirty fibers, only a few fibers are illustrated, to get an idea of the differences in the pathways of the fibers. To see the main differences between apical, middle and basal fibers in more detail, the fibers api1, api4, mid4 and bas7 are taken as representatives and shown in fig. 7.8 to 7.11. The

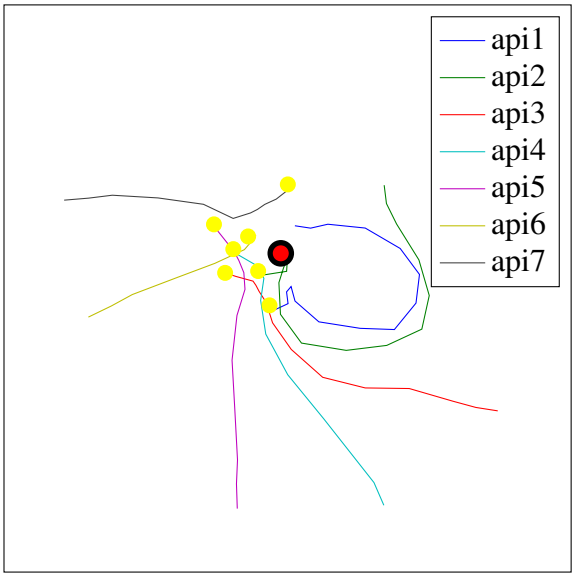

Figure 7.4: Top view regarding to the midmodiolar axis (red circle) on the peripheral processes of the apical fibers and their soma position (yellow circles).

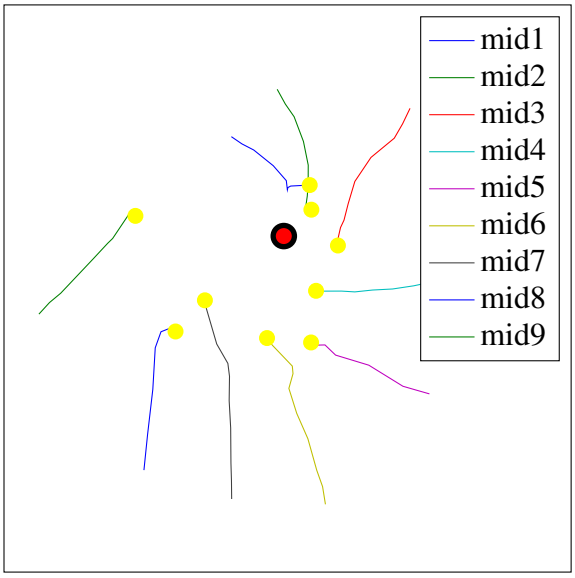

Figure 7.5: Top view regarding to the midmodiolar axis (red circle) on the peripheral processes of the middle fibers and their soma position (yellow circles).

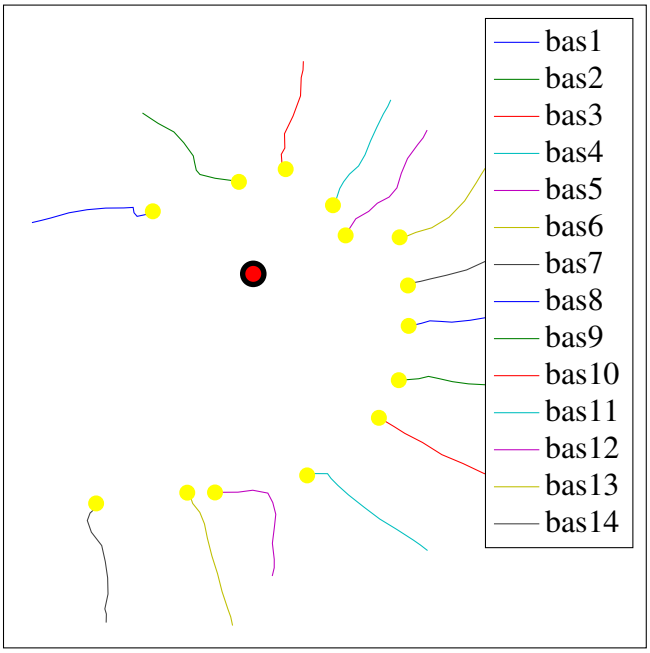

Figure 7.6: Top view regarding to the midmodiolar axis (red circle) on the peripheral processes of the basal fibers and their soma position (yellow circles).

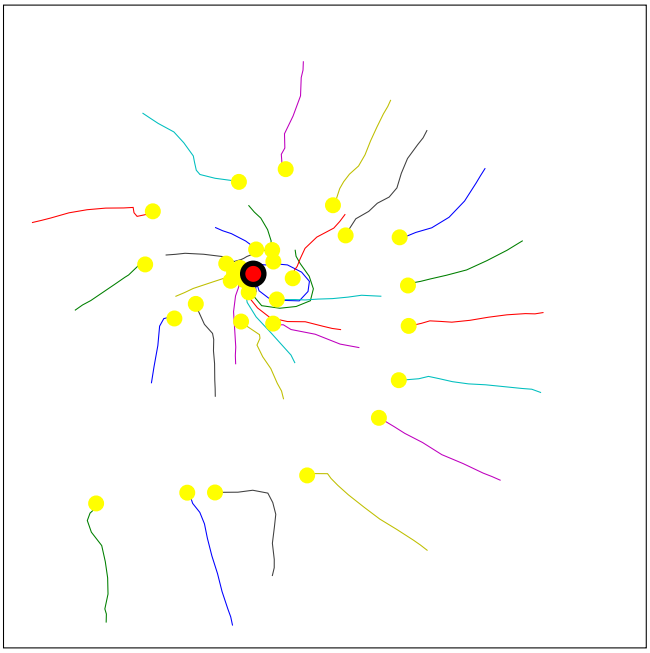

Figure 7.7: Top view regarding to the midmodiolar axis (red circle) on the peripheral processes of all fibers and their soma position (yellow circles).

yellow circles again denote the soma. Note that for reasons of presentation the point of view of fig. 7.8 to 7.11 is completely different to fig. 7.1 and 7.2, where all fibers are shown. Displaying the partially complex 3D structure of the fibers in 2D is difficult. Therefore the figures 7.8a to 7.10a and 7.11 have the same point of view; however, fig. 7.8b to 7.10b have various different points of view to show the unique peculiarities of the respective fibers.

The differences in the pathways of the fibers are remarkable. Both apical fibers show a high spiraling in their pathway. The middle fiber mid4 also shows a coiling. Finally, the basal fiber bas7 shows no spiraling and is more or less planar.

When looking at the three spiraling fibers api1, api4 and mid4 in more detail, several peculiarities are visible: api1 runs through two spirals, whereas one is in the peripheral process and the other in the central axon. The spirals are rather compressed than elongated. This also holds for api4, which has two spirals in the central axon but none in the peripheral process. However, the spiraling of mid4 is very elongated and hardly visible in fig. 7.10a. For all fibers the spiraling has a rather small radius.

The statements about the fiber geometry can be generalized to the other fibers: apical fibers are in general highly spiraling in the central axon. The spiraling is rather on a tight space and partially also in the peripheral process. Furthermore the middle fibers are spiraling to a lower extent only in the central axon and the spirals are highly stretched. However, only the basal fibers show the planar shape, which is usually assumed when modeling SGCs.

Recapitulating the described results reveals, that the differences between realistic fibers and theoretical fibers (as shown in fig. 7.1) are partially tremendously. Only the basal fibers show the more or less planar shape. However, the deviations are mostly in the central axon and not too near the soma; this means it is mainly not at the part of the neuron, which is intended for electrical stimulation. Though, the apical fibers partially show a high spiraling in the peripheral process, which is a possible stimulation site. Furthermore the spiraling in the dendrite of api1 and api2 leads to the effect, that these fibers come near towards multiple electrodes and are therefore stimulated more easily. Hence it is worth investigating the electrical stimulation of the apical fibers.

7.2 Modeling of natural hearing

Besides the geometric pathway of the SGCs, natural hearing was studied. In natural hearing the fibers are stimulated by the inner hair cells at their peripheral ends. This can be modeled by stimulating the first compartment of the specific neuron intra-cellularly.

In our model, all fibers were stimulated at the first compartment with a pulse durating 0.1 ms and having an amplitude of -0.004 μA. Furthermore arrival times of the generated AP at the soma and the end of the neurons were computed.

Clearly the arrival time at the soma corresponds with the length of the peripheral

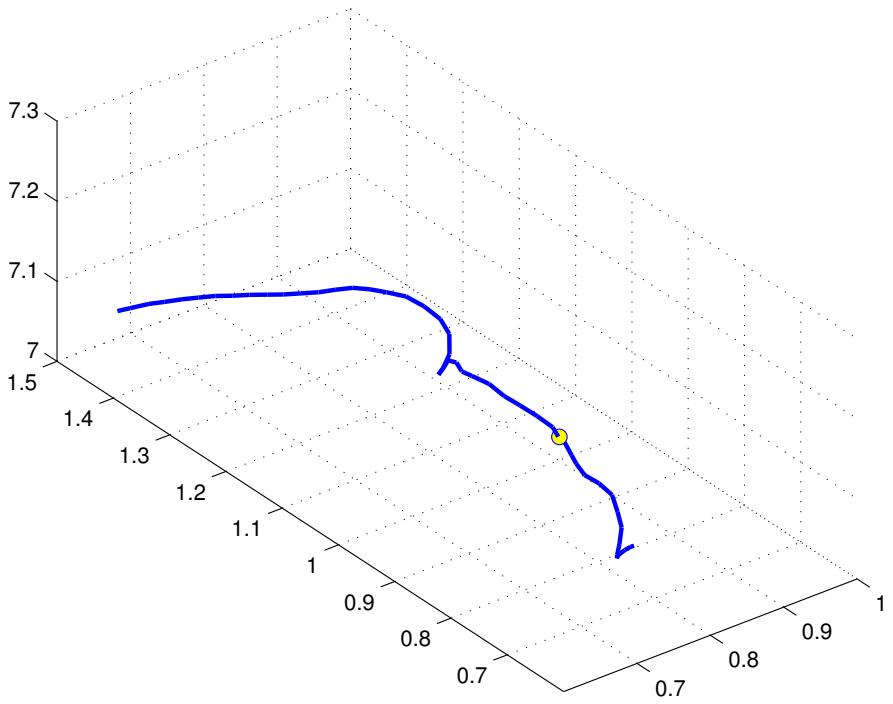

(a) Standard point of view.

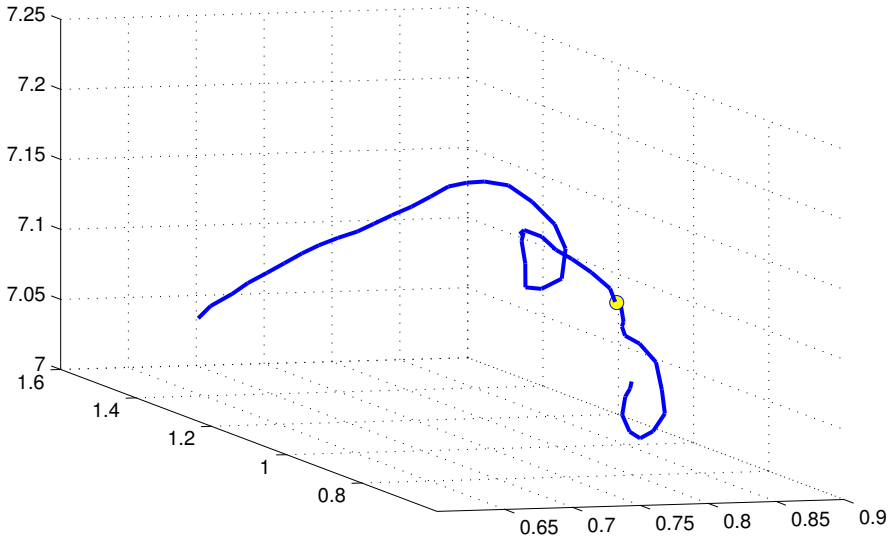

(b) Specific point of view.

Figure 7.8: Presentation of 3D pathway of api1.

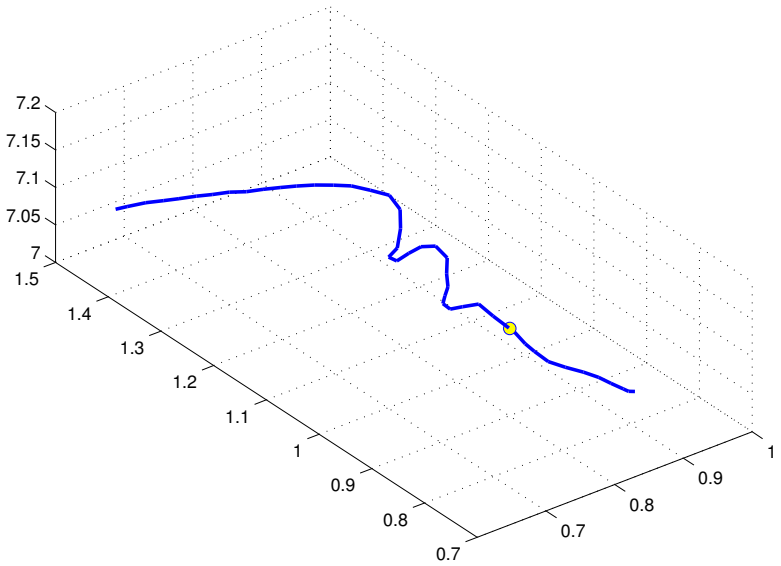

(a) Standard point of view.

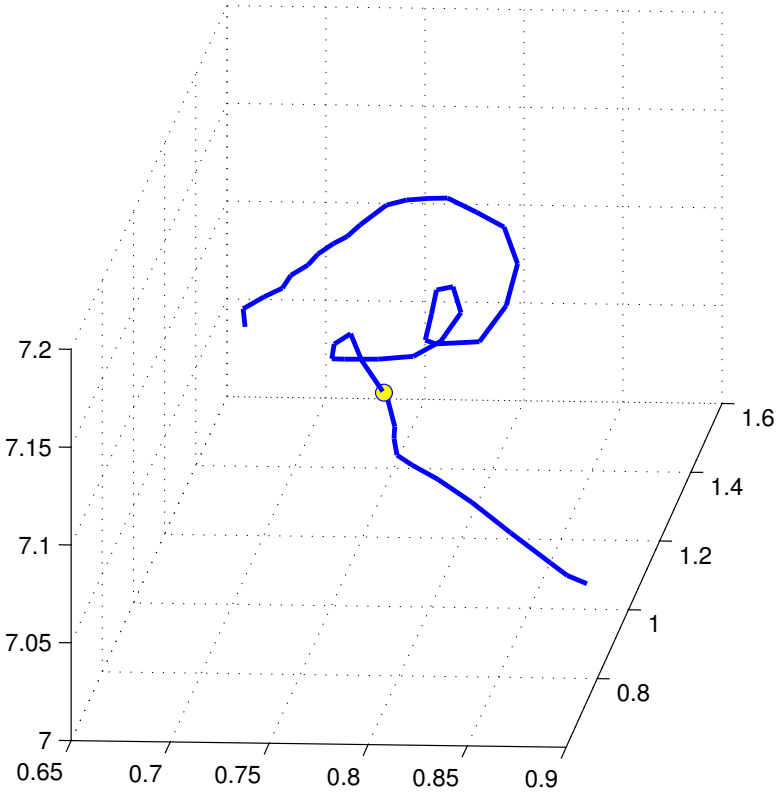

(b) Specific point of view.

Figure 7.9: Presentation of 3D pathway of api4.

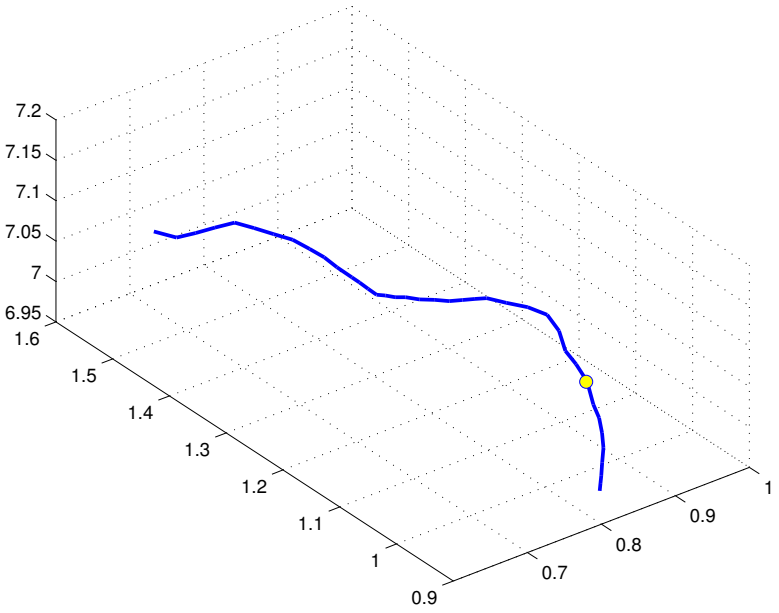

(a) Standard point of view.

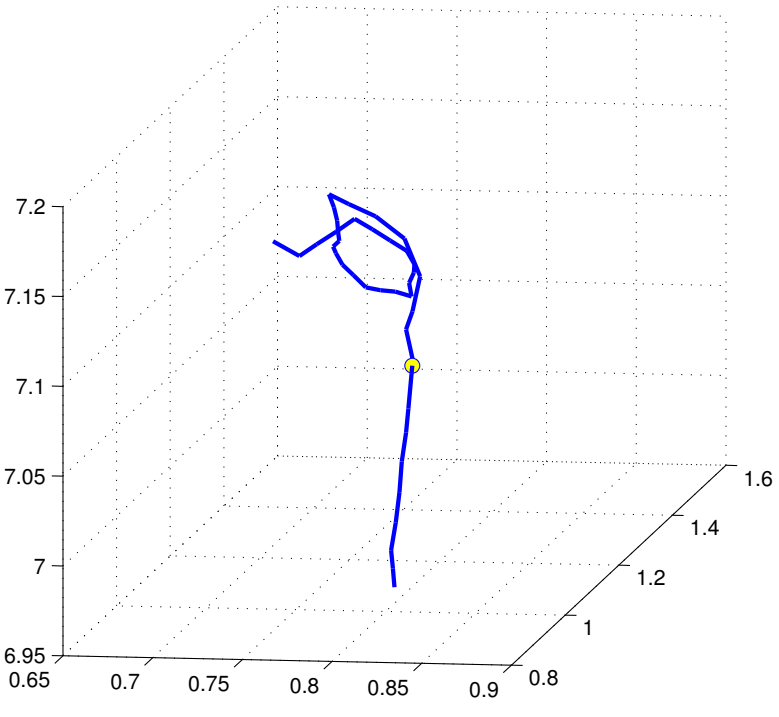

(b) Specific point of view.

Figure 7.10: Presentation of 3D pathway of mid4.

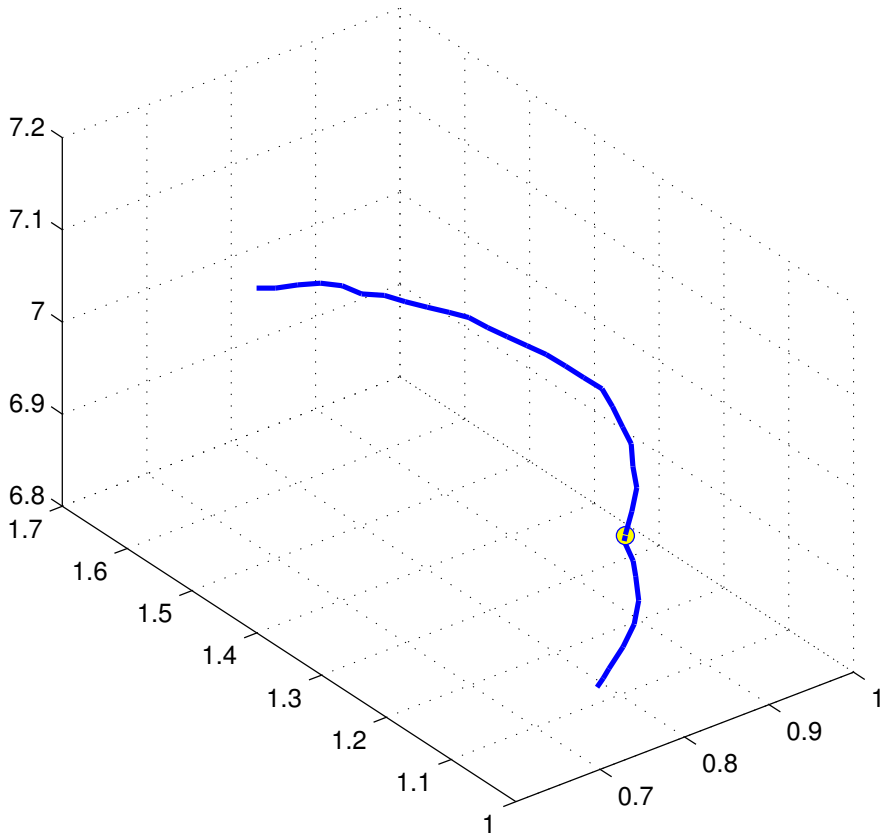

Figure 7.11: Presentation of 3D pathway of bas7, standard point of view.

process. However, since the length of the peripheral internodes differed for the various fibers (as described in chapter 5), it was investigated whether this has a remarkable effect on the arrival time at the soma. Hence arrival time of the AP at the soma and length of the peripheral process were compared. It turned out, that the differences of the internodal length have consequences regarding the arrival time at the soma, but these are only marginal. Therefore one can assume arrival time at the soma and peripheral length corresponding linearly, see fig. 7.12. Hence the effect of the variable peripheral internode length has negligible consequences.

Afterwards the durations of the APs until reaching the soma and the end for all thirty fibers were compared, see fig. 7.13. It shows clearly, that the APs of the apical fibers need longer to arrive at the end than the ones of the middle or basal fibers. Interestingly for the most basal fibers the arrival time is increasing again. The minimum time need the middle fibers. Of course these times depend on the length of the central process. The high spiraling of the apical fibers in the central process is the reason for the greater length of the apical fibers in comparison to the middle fibers.

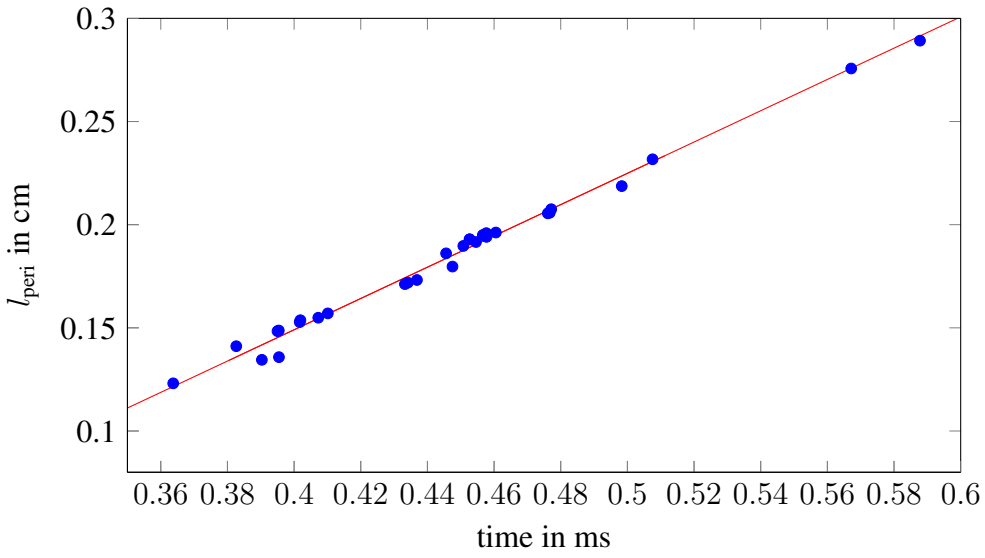

Figure 7.12: Soma time in ms against l_{peri} in cm; data points in blue, best fitting line in red.

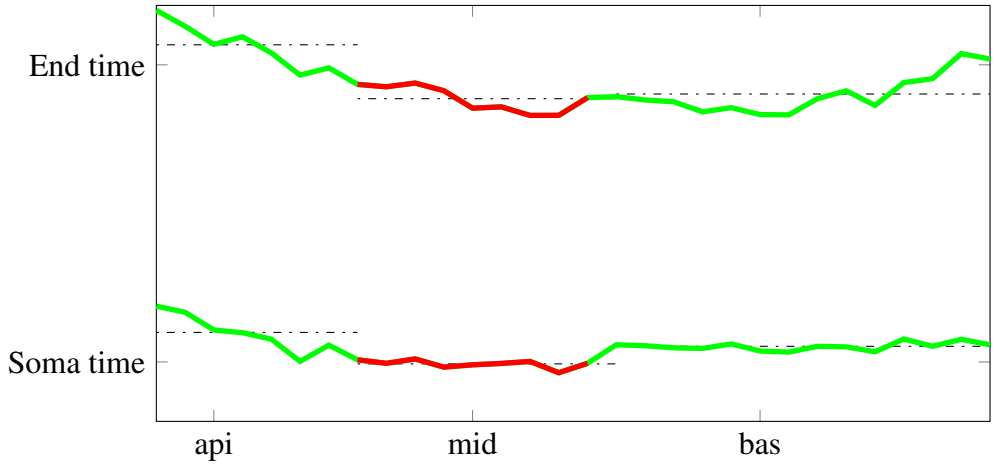

Figure 7.13: Comparison of durations for reaching the soma and the end compartment, for the apical, middle and basal fibers. The dash-dotted lines show the respective mean values of the durations.

The described durations of the APs for reaching the soma respectively the end of the fibers can be assumed as representative durations for natural hearing. This means, they can be compared with the arrival times of extracellular stimulation in the following paragraphs. Consequently it helps comprehending, whether differences in the durations are naturally or not. So one can decide, whether durations of APs for extracellular stimulation are abnormal.

Chapter 8

Study of the apical nerve fibers and apical electrodes

How the spiraling of the apical fibers described in chapter 7 affects their electrical excitability, is the topic of this chapter. For example one interesting question is, whether the tonotopic principle still holds in the apical region of the cochlea. Does the spiraling of the fibers and the corresponding low distance towards multiple electrodes disturb this principle? Another question is which subpopulations can be stimulated simultaneously by the apical electrodes.

The procedure to check this was as follows: for the apical electrodes, as described in chapter 4, the THs of the most sensitive fibers were derived for all four stimulation types ANO, CAT, BIA and BIC. This was separately performed for the normal, healthy and the degenerated fibers - these are fibers with a missing dendrite, thus starting at the soma. Afterwards it was tested which additional fibers are successfully stimulated when increasing the stimulus. The aim of this approach is to find out, whether one can observe a violation of the tonotopic principle (TP) or other remarkable results in the apical region of the cochlea. Note that in the following the most apical electrode EL1 is left out, since it has a reduced radius in comparison to the other electrodes.

8.1 Normal fibers

First of all, for every apical electrode and stimulation type CAT, ANO, BIC and BIA the fiber is evaluated, which needs the lowest current to be stimulated. The results for these most sensitive fibers and their THs are listed in 8.1; for the computation the current was

increased in 0.005 mA steps, therefore partially more than one fiber is listed.

Table 8.1: Most sensitive fibers and thresholds in mA for stimulation type and electrode.

Electrode	**CAT fiber**	**TH**	**ANO fiber**	**TH**	**BIC fiber**	**TH**	**BIA fiber**	**TH**
EL2	api1	0.03	api1	0.03	api1	0.03	api1	0.035
EL3	api1	0.03	api1	0.035	api1	0.04	api1, api3	0.045
EL4	api1	0.05	api1	0.045	api5	0.055	api1	0.06
EL5	api1	0.04	api1, api5	0.055	api1, api5	0.05	api1	0.05
EL6	api1	0.04	api5	0.045	api5	0.04	api5	0.045
EL7	api1, api4, api5	0.045	api5	0.045	api5	0.045	api5	0.05
EL8	api4-api7	0.045	api7	0.045	api7	0.04	api5, api7	0.05
EL9	api5	0.04	api7	0.045	api7	0.04	api7	0.045
EL10	api5, api7	0.045	api7	0.045	api7	0.04	api7	0.045
EL11	api6, api7	0.04	mid1	0.04	api6, mid1	0.04	api6	0.045
EL12	api6	0.035	mid1	0.045	api6	0.04	api6	0.04

It is eye-catching, that the most sensitive fiber for an electrode is not necessarily the same for all four stimulation types. So for the most apical electrode EL2 only api1 is the most sensitive fiber for all stimulation types. However, the most sensitive fibers for EL4 to EL6 are two fibers, which are non-neighboring, namely api1 and api5. In contrast to this, for EL11 we have the neighboring fibers api6 to mid1 most easily stimulated. This means, under certain circumstances, changing the stimulation type can have great consequences. The THs lay between 0.03 mA, e.g. for (EL2 CAT), and 0.06 mA for (EL4, BIA). However, in most cases the THs are between 0.04 mA and 0045 mA.

Another remarkable fact is, that partially more than one fiber is the most sensitive one. In most cases these fibers are more or less neighboring. For example EL11 has api6 and api7 as most sensitive fibers for a CAT stimulus. However, for (EL5, ANO), (EL5, BIC) and (EL7, CAT) clearly non-neighboring fibers are stimulated at once, namely api1 and api5; for (EL7, CAT) also api4. This means, the tonotopic principle is violated. As mentioned later, this also occurs partially for a higher stimulation current. This is elaborated more precisely later in a separate paragraph.

Now it was checked what happens, when the stimulation current is increased; for all electrodes and stimulation types the stimulus amplitudes were set to 125%, 150% and to 200% of the THs to get a first view on the populations of the additionally stimulated fibers. The stimulated fibers are given in table 8.2. In special cases further stimulus amplitudes were investigated to get more detailed information about the stimulated sub-populations.

Table 8.2: Stimulated fibers when setting electrode current to 125%, 150% and 200% of the corresponding threshold of table 8.1.

Electrode	**Factor**	**CAT**	**ANO**	**BIC**	**BIA**
EL2	1.25	api1	api1	api1, api2	api1, api2
	1.5	api1, api3	api1, api2	api1, api2	api1-api3
	2	api1-api4	api1, api2	api1-api3	api1-api3
EL3	1.25	api1	api1, api2	api1-api3	api1-api3
	1.5	api1-api3	api1, api2	api1-api4	api1,-api3
	2	api1-api4	api1, api2	api1-api5	api1-api5
EL4	1.25	api1, api5	api1	api1, api4, api5	api1, api2, api5
	1.5	api1-api6	api1, api2	api-api5	api1-api5
	2	api1-api7	api1-api5	api1-api7	api1-api6
EL5	1.25	api1	api1, api4, api5	api1, api5	api1, api5
	1.5	api1-api6	api1-api5	api1-api5, api7	api1-api5
	2	api1-api7	api1-api7	api1-api7	api1-api7
EL6	1.25	api1-api6	api5	api1, api5	api1, api4, api5
	1.5	api1-api7	api1, api3-api5	api1, api3-api5, api7	api1-api6
	2	api1-api7	api1-api7	api1-api7	api1-api7
EL7	1.25	api1-api7	api5, api7	api3, api5, api7	api3-api7

Continued on next page

Table 8.2 – continued from previous page

Electrode	Factor	CAT	ANO	BIC	BIA
	1.5	api1-api7	api3-api7	api1, api3-api7	api1-api7
	2	api1-mid1	api1-api7	api1-mid1	api1-api7
EL8	1.25	api1-api7	api5-api7	api5, api7	api4-api7
	1.5	api1-api7	api4-api7	api3-api5, api7	api3-api7
	2	api1-mid2	api1,api3-mid1	api1-mid1	api1-mid1
EL9	1.25	api3-api7	api5-api7	api7	api5, api7
	1.5	api2-api7	api4-api7	api4-mid1	api4-api7
	2	api1-mid2	api1,api3-mid1	api3-mid2	api3-mid1
EL10	1.25	api3-mid1	api3-mid1	api7, mid1	api5, api7
	1.5	api2-mid2	api2-mid2	api5-mid2	api4-mid1
	2	api1-mid2	api1-mid2	api3-mid2	api3-mid2
EL11	1.25	api5-mid2	api7, mid1	api6-mid2	api6-mid1
	1.5	api3-mid2	api7, mid1	api6-mid2	api5-mid2
	2	api2-mid2	api5-mid1	api4-mid2	api4-mid2
EL12	1.25	api6-mid2	api7-mid2	api6,mid1,mid2	api6
	1.5	api6-mid2	api7-mid2	api6-mid2	api6-mid2
	2	api4-mid3	api5-mid2	api6-mid3	api6-mid2

It turned out, that the two most apical electrodes are able to stimulate the fibers api1 to api3, and even up to api5, in most cases sequentially. This means, a well-defined, enclosed subpopulation can be stimulated. However, the following electrodes EL4 to EL6, for a CAT stimulus also EL7, show the already known peculiarity: for certain stimulus amplitudes and stimulation types the cases of a stimulation of (api1, api5), (api1, api2, api5) or (api1, api4, api5) happens. This means a subpopulation of clearly non neighboring. fibers is stimulated - so the tonotopic principle is violated. This peculiarity is investigated in an separate, following paragraph in more detail. The next electrodes EL7 to EL9 can stimulate subpopulations of api1-api7 or api3-api7 under certain circumstances, whereas the target fibers of EL10 to EL12 range partially from api5 to mid2.

A method for avoiding the described simultaneous stimulation of only non neighboring. fibers for the electrodes EL4 to EL6, is to decrease or to increase the current. Decreasing the current leads finally to a stimulation of only one fiber - in our case either api1 or api5. However, both fibers can be stimulated alone (or in a greater subpopulation

of e.g. api1-api3 resp. api5-api7) by more apical resp. more basal located electrodes. The other option of increasing the current leads to an activation of all the fibers between api1 and api5, and therefore to a quite big subpopulation - but this can also be stimulated by the most apical electrodes EL2 and EL3. This means, the electrodes EL4 to EL6 are actually redundant.

The extreme case of stimulating all seven apical fibers is possible for electrodes EL2 to EL8, so between $870°$ and $690°$. However, stimulating only single fibers is not that easy. Although the electrodes of the model have a distance of only $30°$, e.g. api3 and api4 can not be stimulated alone. This means even more electrodes would have to be implanted, when intending an individual stimulation of all fibers. Interestingly it is further difficult to stimulate every thinkable neighboring. subpopulation, like for example (api3, api4, api5).

An possible example would be a wished stimulated subpopulation size of three to four fibers per electrode. In fig. 8.1 a top view on the apical electrodes and dendrites of the fibers api1 to mid2 are displayed. Electrodes and fibers are given in the same color, when the fibers belong to a possibly stimulated subpopulation of the electrode. So for example api1 to api3 can be stimulated by EL2 and EL3. The electrodes EL4 to EL6 are marked in white, since these are the ones sensitive for the violation of the TP and no neighboring. subpopulation of three to four fibers can be stimulated by them. Therefore these are left out. EL7 to EL10 can stimulate api4-api7; EL11 and EL12 can stimulate a subpopulation of api6 to mid2. Since the subpopulations of EL7-EL10 and EL11-EL12 are overlapping towards api6 and api7, these two fibers are marked in green.

In summary, it is easy to stimulate specific subpopulations like api1 to api3, api3 to api7 or api5 to mid2. However, a stimulation of only api3 to api5 happens rarely. Also the individual stimulation of every fiber is not possible. Furthermore there is the special case of a simultaneous stimulation of api1 and api5. This case represents a violation of the tonotopic principle, since only non-neighboring fibers are stimulated at once. This peculiarity is analyzed in more detail in the following paragraph.

Description of the violation of the tonotopic principle

As described above, partially the case of a simultaneous stimulation of (api1,api5), (api1,api2,api5) or (api1,api4,api5) occurs. The reason for this peculiarity, it's characteristics and it's consequences are described in short in this paragraph.

The violation of the TP occurs for electrodes EL4 to EL7, so between $720°$ and $810°$. All the cases are listed in table 8.3 with electrode and stimulus type and threshold amplitude of the four electrodes. It is remarkable, that this peculiarity does not occur for every stimulation mode. So it happens for ANO, BIC and BIA for the electrodes 4,5, and 6, whereas a CAT stimulus elicits it only for electrodes 4 and 7. The range of current, where the TP violation happens, was not evaluated systematically. However, the range is not too big, since as listed in table 8.2, for 150% of the TH this peculiarity

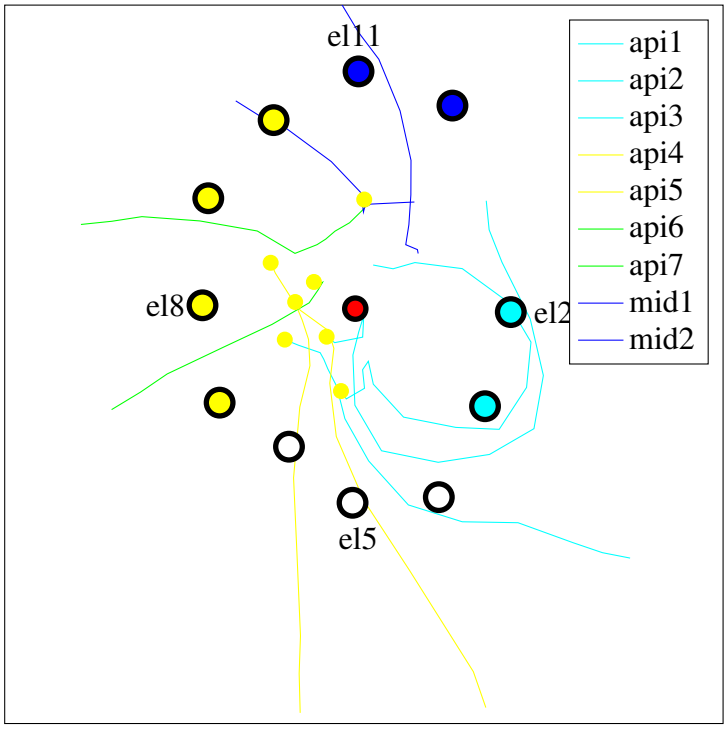

Figure 8.1: Top view regarding to the midmodiolar axis (small, red circle) on peripheral processes of api1-mid2 with soma (small yellow circles) and electrodes (big circles). Corresponding fibers and electrodes are displayed in the same color, except for api6 and api7, which belong to both the yellow and the blue population.

does not occur any longer. It is noticeable, that there are partially big differences in the ISs in the eleven cases. For example for (EL4, ANO) the three fibers api1, api2 and api5 are all stimulated at the first compartment. However, in most cases the ISs of the simultaneously stimulated fibers are quite different. For example for (EL4, CAT) we have compartment 15 (the presomatic compartment) for api1 and compartment 7 for api5 as sites of initiation.

The reason for the peculiarity of the violation of the tonotopic principle is the following: as illustrated roughly in fig. 6.3 and already mentioned above, the high spiraling of api1 and api2 causes a partially low distance towards various electrodes, more precisely to EL2 to el6. For example fig. 6.4b shows a very small distance of the peripheral process of api1 and api2 towards EL5 before the soma. This small distance promotes the high external potential of api1 for el5, as pictured in fig. 6.5b and therefore the likelihood of being stimulated with a relatively low stimulus amplitude. However, also api5 has a low distance towards EL5 for about two thirds of it's dendrite. Furthermore it's V_e shows a certain peak as well as it's membrane potential. This means, that api1 (and

Table 8.3: Thresholds in mA and initiation sites for cases of a simultaneous stimulation of non-neighboring fibers.

Electrode	Stimulation type	Stimulation Amplitude in mA	Fibers	IS
EL4	CAT	0.06	api1	15
			api5	7
	ANO	0.075	api1	1
			api2	1
			api5	1
	BIC	0.065	api1	15
			api4	1
			api5	5
	BIA	0.07	api1	1
			api5	7
EL5	ANO	0.055	api1	1
			api5	1
	BIC	0.05	api1	15
			api5	5
	BIA	0.055	api1	15
			api5	7
EL6	ANO	0.06	api1	1
			api4	17,19
			api5	5
	BIC	0.05	api1	15
			api5	5
	BIA	0.05	api1	15
			api5	7
EL7	CAT	0.045	api1	15
			api4	11
			api5	11

sometimes api2) as well as api5 (and sometimes api4) have a low distance towards EL4 to EL7. They all also have high potential along V_e for these electrodes and also a higher excitability than the other fibers. The violation of the TP therefore directly results from the high dendritic spiraling of api1 (and api2).

An example for the simultaneous stimulation of api1 and api5 is (EL5, BIC, 0.05 mA). As given in table 8.3 and shown in fig. 8.2, the initiation sites are completely different: whereas api5 is stimulated at compartment 5 - this means near the peripheral end - api1 is stimulated at compartment 15, the presomatic compartment. The discrepancy between both initiation sites results from the pathway (and therefore from the electrode distance) of both fibers: whereas the fiber api5 is near towards EL5 for about two thirds of it's peripheral process, api1 has a low distance shortly before and around the soma.

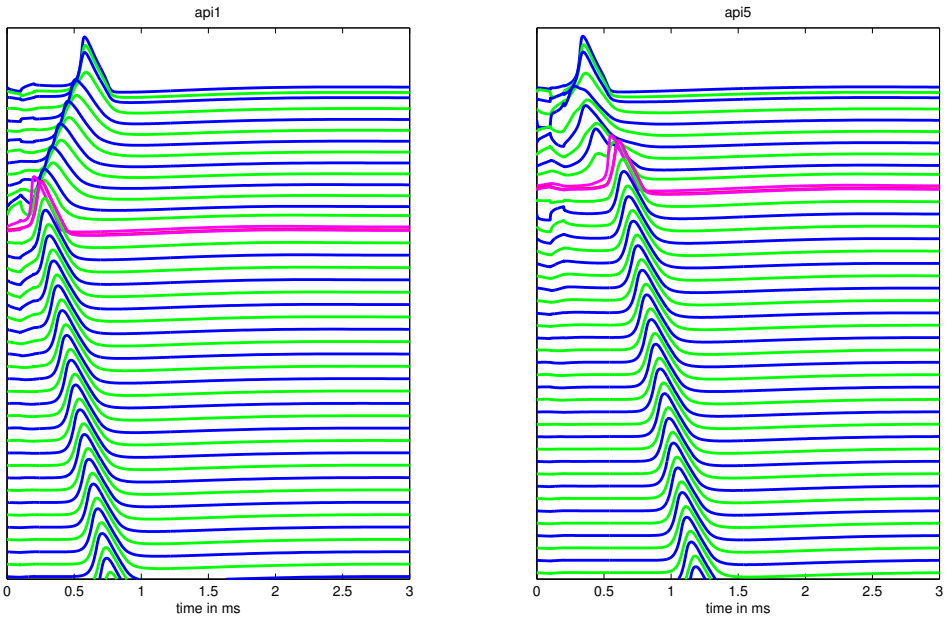

Figure 8.2: Excitation profile of api1 and api5 for a 0.05 mA BIC stimulus of EL5. The soma region (pre- and postsomatic compartment, as well as the soma) is given in magenta.

A further result displayed in fig. 8.2 is that the AP of api1 reaches the end earlier than the AP of api5. Hence we have in our example $t_{\text{end,api1}} = 1.2317ms$ and $t_{\text{end,api5}} = 1.5749ms$. This means the duration of the AP until reaching the end of api5 is about a third longer than the duration of the AP of api1. This large discrepancy comes mainly from the fact, that api5 is stimulated more peripherally than api1. Therefore the AP of api5 has to travel along a longer way. However, as described in chapter 7.2, the durations until reaching the end in natural hearing are $t_{\text{end,api1,nat}} = 1.5835$ and $t_{\text{end,api5,nat}} = 1.4402$. This means, the discrepancy is naturally much smaller. Furthermore in natural hearing

the duration for api1 is longer than the one of api5 - contrary to the durations of our example case. Similar results hold for the other cases, when the ISs of the stimulated fibers are quite apart.

Recapitulating the described details, a violation of the TP can occur for electrodes placed between $720°$ and $810°$ in the cochlea. However, the range of stimulating current, where it occurs is limited and lays between the TH and 150 % of the TH. Furthermore this violation happens for biphasic as well as monophasic stimulation. The violation of the TP directly results from the high spiraling of the dendrite of api1 (and api2). Furthermore the highly differing ISs of the simultaneously stimulated fibers lead to deviations of t_{end} in comparison to the natural hearing described in chapter 7.2 of.

8.2 Degenerated fibers

The previous results only hold for normal, undamaged fibers. However, as mentioned in chapter 2, there is the possibility, that the neuron fibers are degenerated; this means the SGCs lack a peripheral process and start right from the soma. This section summarizes the results of the stimulation of the degenerated fibers.

First of all, as for the healthy fibers, THs and most sensitive (now degenerated) fibers for every electrode were computed; the results are listed in table 8.4. Again the stimulation current was increased in 0.005 mA steps, which leads partially to multiple most sensitive fibers for an electrode and stimulation type.

However, the results seem strange, since for almost every electrode and stimulation type the fiber api5 is the most sensitive one. Exceptions are mainly EL2 to EL8 with a CAT stimulus (and api3 as most sensitive fiber), or EL11 and EL12 for all stimulation modes (with api6 or api7 as most sensitive fibers).

In the following, the reason for this is elaborated: as displayed in fig. 6.5, V_e is partially quite similar for all fibers in the central axon. This holds especially for the more apical electrodes EL2 and EL5 in fig. 6.5a and 6.5b. However, the courses of V_e of api4 and api5 are special, since both have two very sharp bends right after the soma, whereas the other fibers show a much smoother V_e.

When further looking at fig. 6.7, it becomes clear, that these sharp bends do have remarkable consequences: the sharp bends of V_e of api4 and api5 cause partially strong hyper- and depolarizations on the membrane along the fibers. This means, these fibers are very likely to be stimulated easily right after the soma. This holds for api5 even more than for api4, and hence the results of table 8.4 are no longer surprising. However, it is doubtful, whether the sharp bends are really realistic or just an regrettable artifact with major consequences.

Despite the dubious results for the most sensitive fibers, the TH was increased to find out, which additional fibers can be stimulated easily by the electrodes. Since the THs are overall quite big (especially for the more apical electrodes) the currents were

Table 8.4: Most sensitive degenerated fibers and thresholds in mA for stimulation type and electrode.

Electrode	**CAT fiber**	**TH**	**ANO fiber**	**TH**	**BIC fiber**	**TH**	**BIA fiber**	**TH**
EL2	api3	0.085	api5	0.13	api5	0.105	api5	0.13
EL3	api3	0.075	api5	0.11	api5	0.09	api5	0.11
EL4	api2, api3	0.065	api3-api5	0.095	api5	0.075	api4, api5	0.095
EL5	api3	0.055	api4, api5	0.075	api4, api5	0.065	api4, api5	0.08
EL6	api3	0.05	api4, api5	0.065	api5	0.055	api5	0.065
EL7	api3, api5	0.05	api5	0.06	api5	0.055	api5	0.06
EL8	api3, api5	0.05	api5	0.055	api5	0.05	api5	0.06
EL9	api5	0.05	api5	0.055	api5	0.05	api5	0.06
EL10	api5-api7	0.055	api5	0.065	api5	0.055	api5, api6	0.065
EL11	api6	0.04	api7	0.07	api6	0.045	api6	0.045
EL12	api6	0.035	api7	0.07	api6	0.04	api6	0.04

set to 106.25%, 125% and 150% of the corresponding TH of table 8.4. It turned out, that a stimulation of the subpopulations (api3, api4, api5), (api5, api6, api7) and (api6, api7, mid1) is generally possible. However, only for a CAT stimulus a stimulation of (api1, api2, api3) is possible. Of course, the reason for this is the easy stimulation of api5. Deviations of the TP as in the case of long fibers were not observed.

Chapter 9

Discussion and comprehension

In this chapter some of the results of the proceeding chapters are recapitulated and discussed. First of all it is summed up, how trustworthy and correct the model described in chapter 4 and 5 is. Afterwards the reliability and the meaning of the partially observed violation of the tonotopic principle in chapter 8 is discussed.

9.1 Correctness of the model

The model described in this thesis is a tool for predicting the electrical stimulation of fibers. However, a computer simulation does not claim to be absolutely correct. But, despite several weaknesses, which are listed in the following, the described model is much more realistic than older ones. For example in [Rattay et al., 2001a] or [Wenger, 2012] the external potential V_e was calculated for a homogeneous tissue. Furthermore in [Rattay et al., 2001b], where a simplified cochlear geometry was considered as well as the inhomogeneity of the tissue, the fine structure of the cochlea and the realistic pathway of fibers were not featured. However, for a better understanding and evaluation of the results of the simulation, it is necessary to know about the weaknesses of the model. Some of them are described in the following, by also mentioning their importance and possibilities how to avoid them.

As described in chapter 4, the geometry of the cochlea-surrounding tissue as well as it's material values were quite arbitrary. Moreover, the grounding also could have defined differently, for example by a reference electrode. Also the material values assigned to the various geometric components are might not absolutely correct. Consequences of changing the outer geometry, it's material and the grounding were not evaluated sys-

tematically in this thesis. But it is thinkable, that it has rather an influence on the range of V_e, but not too big consequences on qualitative course of V_e at the beginning of the fibers, which are possible sites of initiation of APs. So rather the exact values of the THs than the ISs are probably influenced by the outer geometry and grounding. The sensitivity of the model towards the electrical conductivities σ was tested in chapter 6.1. It turned out, that the model does not react too sensitive towards changing these values regarding to the THs as well as the ISs.

As also described in chapter 6.1, the fibers are partially going through geometric components of the cochlea, which they are actually not intended to pass. Reasons for this are factors like the actually small distance of the fibers towards these components, the limited resolution of the μCT and labor-extensive segmentation. However, it is also noted, that this phenomenon overall has only little consequences for V_e; but it partially leads to sharp bends and discontinuities of V_e, with might bad consequences, as described later. Avoiding this imprecision would probably be combined with a lot of work and should be done with the already interpolated fibers.

The very interpolation of the fibers when transforming them into a compartment chain, has impact on the pathways, as described in chapter 5, and on the external potential V_e, as explained in chapter 6.1. Whereas it's influences on the pathway are rather ignorable, might peaks of V_e are lost by the interpolation. But solving this manually would be quite elaborate.

The described unsmoothness of V_e and the many discontinuities can cause APs, see chapter 6.2. As described in chapter 8.2, especially the short fibers are obviously a victim of the sharp bends of V_e: api4 and api5 have both sharp bends after the soma for multiple electrodes. Therefore these two fibers are most easily stimulated by a lot of electrodes. Possibly a smoothing of V_e could solve this, but it would be laborious.

Finally, the Hodgkin-Huxley compartment model is of course also a model with weaknesses. So the implementation of the ion channels is might not correct, e.g. due to the missing information of the correct ion channel density. Furthermore, as described in chapter 5, there was the tendency of APs generated at the last compartment for anodic stimulation. This was solved by the artificial elongation of the fibers.

9.2 Consequences of the phenomenon of the partial violation of the tonotopic principle

As mentioned above, the model has some weaknesses, but still helps a lot when studying the excitability of neurons by electrodes. In chapter 8, the relationship between the apical fibers and apical electrodes concerning the tonotopic principle was studied.

The apical electrodes were placed in the ST between $570°$ and $900°$. As described in chapter 2, the length of nowadays CIs is limited. No electrode array reaches up

to the apex, since the coiled structure of the cochlea makes a harmless implantation difficult. However, the structure of the most apical fibers is very special, since they are partially spiraling as described in chapter 7. This means they differ enormously from the usually assumed planar shape. Therefore it is interesting to investigate, which effect this spiraling might has for electrical stimulation. This also holds, when thinking about the possibility of spiraling middle or basal fibers in other cochleae. Therefore the possibility of setting electrodes at any position is a great advantage of a computer simulation.

One can not expect the results of chapter 8 being absolutely correct. However, the prediction of a violation of the TP by simultaneous stimulation of e.g. only api1 and api5 seems reasonable, when thinking of the special pathway of api1, which comes near to multiple electrodes. Furthermore the phenomenon does not happen only once, but occurs for the electrodes between $720°$ and $810°$ in our model. Moreover, it partially happens for all four stimulation types.

When thinking about really placing electrodes also in the apical region of the cochlea, it would not be too improbable that the phenomenon of the TP could occur: in the described model, the violation of the TP occurs also for a biphasic stimulation; this is preferred in nowadays realistic stimulation for avoiding a might harmful accumulation of currents. Furthermore in the model there is a large range of at least $90°$, which is sensitive for a violation of the TP. This means it might would have to be considered when planning a full insertion of electrode arrays in the cochlea, that special geometric peculiarities can have major consequences for the stimulation strategies.

Bibliography

Adunka, O. and Kiefer, J. (2006). Impact of electrode insertion depth on intracochlear trauma. *Otolaryngology-Head and Neck Surgery*, 135(3):374–382.

Ashmore, J. (2008). Cochlear outer hair cell motility. *Physiological Reviews*, 88(1):173–210.

Biedron, S., Westhofen, M., and Ilgner, J. (2009). On the number of turns in human cochleae. *Otology & Neurotology*, 30(3):414–417.

Blamey, P., Artieres, F., Başkent, D., Bergeron, F., Beynon, A., Burke, E., Dillier, N., Dowell, R., Fraysse, B., Gallégo, S., et al. (2012). Factors affecting auditory performance of postlinguistically deaf adults using cochlear implants: An update with 2251 patients. *Audiology and Neurotology*, 18(1):36–47.

Bossetti, C. A., Birdno, M. J., and Grill, W. M. (2008). Analysis of the quasi-static approximation for calculating potentials generated by neural stimulation. *Journal of neural engineering*, 5(1):44.

Finley, C. C., Wilson, B. S., and White, M. W. (1990). Models of neural responsiveness to electrical stimulation. In *Cochlear implants*, pages 55–96. Springer.

Fu, Q.-J. and Galvin III, J. J. (2008). Maximizing cochlear implant patients' performance with advanced speech training procedures. *Hearing research*, 242(1):198–208.

Gantz, B. J., Turner, C., Gfeller, K. E., and Lowder, M. W. (2005). Preservation of hearing in cochlear implant surgery: Advantages of combined electrical and acoustical speech processing. *The Laryngoscope*, 115(5):796–802.

Hinojosa, R. and Marion, M. (1983). Histopathology of profound sensorineural deafness. *Annals of the New York Academy of Sciences*, 405(1):459–484.

Hochmair, I., Arnold, W., Nopp, P., Jolly, C., Muller, J., and Roland, P. (2003). Deep electrode insertion in cochlear implants: Apical morphology, electrodes and speech perception results. *Acta oto-laryngologica*, 123(5):612–617.

Hochmair, I., Nopp, P., Jolly, C., Schmidt, M., Schößer, H., Garnham, C., and Anderson, I. (2006). MED-EL cochlear implants: State of the art and a glimpse into the future. *Trends in amplification*, 10(4):201–219.

Hodgkin, A. L. and Huxley, A. F. (1952). A quantitative description of membrane current and its application to conduction and excitation in nerve. *The Journal of physiology*, 117(4):500.

Hughes, M. L. and Abbas, P. J. (2006). Electrophysiologic channel interaction, electrode pitch ranking, and behavioral threshold in straight versus perimodiolar cochlear implant electrode arrays. *The Journal of the Acoustical Society of America*, 119:1538.

Izzo, A. D., Suh, E., Pathria, J., Walsh, J. T., Whitlon, D. S., and Richter, C.-P. (2007). Selectivity of neural stimulation in the auditory system: A comparison of optic and electric stimuli. *Journal of biomedical optics*, 12(2):021008–021008.

Javel, E. and Shepherd, R. K. (2000). Electrical stimulation of the auditory nerve: III. Response initiation sites and temporal fine structure. *Hearing research*, 140(1):45–76.

Ketten, D. R., Skinner, M. W., Wang, G., Vannier, M. W., Gates, G. A., and Neely, J. G. (1998). In vivo measures of cochlear length and insertion depth of nucleus cochlear implant electrode arrays. *Ann Otol Rhinol Laryngol*, 107(1):1B11.

Klepfer, R. N., Johnson, C. R., and Macleod, R. S. (1997). The effects of inhomogeneities and anisotropies on electrocardiographic fields: A 3-D finite-element study. *Biomedical Engineering, IEEE Transactions on*, 44(8):706–719.

Kosterich, J. D., Foster, K. R., and Pollack, S. R. (1983). Dielectric permittivity and electrical conductivity of fluid saturated bone. *Biomedical Engineering, IEEE Transactions on*, (2):81–86.

Lazard, D. S., Vincent, C., Venail, F., Van de Heyning, P., Truy, E., Sterkers, O., Skarzynski, P. H., Skarzynski, H., Schauwers, K., O'Leary, S., et al. (2012). Pre-, per-and postoperative factors affecting performance of postlinguistically deaf adults using cochlear implants: A new conceptual model over time. *PloS one*, 7(11):e48739.

Lorens, A., Zgoda, M., Obrycka, A., and Skarżynski, H. (2010). Fine structure processing improves speech perception as well as objective and subjective benefits in pediatric MED-EL COMBI 40+ users. *International journal of pediatric otorhinolaryngology*, 74(12):1372–1378.

Luo, X., Fu, Q.-J., and Galvin, J. J. (2007). Vocal emotion recognition by normal-hearing listeners and cochlear implant users. *Trends in Amplification*, 11(4):301–315.

Pfingst, B. E. and Xu, L. (2004). Across-site variation in detection thresholds and maximum comfortable loudness levels for cochlear implants. *Journal of the Association for Research in Otolaryngology*, 5(1):11–24.

Plonsey, R. (2000). Volume conductor theory. In Bronzino, J., editor, *The Biomedical Engineering Handbook: Second Edition.* CRC Press.

Potrusil, T., Wenger, C., Glueckert, R., Schrott-Fischer, A., and Rattay, F. (2012). Morphometric classification and spatial organization of spiral ganglion neurons in the human cochlea: Consequences for single fiber response to electrical stimulation. *Neuroscience*, 214:120–135.

Rask-Andersen, H., Liu, W., Erixon, E., Kinnefors, A., Pfaller, K., Schrott-Fischer, A., and Glueckert, R. (2012). Human cochlea: Anatomical characteristics and their relevance for cochlear implantation. *The Anatomical Record*, 295(11):1791–1811.

Rattay, F. (1998). Analysis of the electrical excitation of CNS neurons. *Biomedical Engineering, IEEE Transactions on*, 45(6):766–772.

Rattay, F. (1999). The basic mechanism for the electrical stimulation of the nervous system. *Neuroscience*, 89(2):335–346.

Rattay, F., Lutter, P., and Felix, H. (2001a). A model of the electrically excited human cochlear neuron: I. Contribution of neural substructures to the generation and propagation of spikes. *Hearing research*, 153(1):43–63.

Rattay, F., Leao, R. N., and Felix, H. (2001b). A model of the electrically excited human cochlear neuron. II. Influence of the three-dimensional cochlear structure on neural excitability. *Hearing research*, 153(1):64–79.

Rattay, F., Greenberg, R., and Resatz, S. (2003). Neuron modeling. In Finn, W. and LoPresti, P., editors, *Handbook of Neuroprosthetic Methods.*, pages 39–73. CRC Press.

Roth, B. J. (2000). The electrical conductivity of tissues. In Bronzino, J., editor, *The Biomedical Engineering Handbook: Second Edition.* CRC Press.

Sato, H., Sando, I., and Takahashi, H. (1991). Sexual dimorphism and development of the human cochlea: Computer 3-D measurement. *Acta oto-laryngologica*, 111(6):1037–1040.

Shapiro, M. G., Homma, K., Villarreal, S., Richter, C.-P., and Bezanilla, F. (2012). Infrared light excites cells by changing their electrical capacitance. *Nature communications*, 3:736.

Skinner, M. W., Holden, T. A., Whiting, B. R., Voie, A. H., Brunsden, B., Neely, J. G., Saxon, E. A., Hullar, T. E., Finley, C. C., et al. (2007). In vivo estimates of the position of advanced bionics electrode arrays in the human cochlea. *The Annals of otology, rhinology & laryngology. Supplement*, 197:2.

Smith, Z. M., Delgutte, B., and Oxenham, A. J. (2002). Chimaeric sounds reveal dichotomies in auditory perception. *Nature*, 416(6876):87–90.

Snyder, R. L., Middlebrooks, J. C., and Bonham, B. H. (2008). Cochlear implant electrode configuration effects on activation threshold and tonotopic selectivity. *Hearing research*, 235(1):23–38.

Spahr, A. J., Dorman, M. F., and Loiselle, L. H. (2007). Performance of patients using different cochlear implant systems: Effects of input dynamic range. *Ear & Hearing*, 28(2):260–275.

Tian, Q., Linthicum, F. H., and Fayad, J. N. (2006). Human cochleae with three turns: An unreported malformation. *The Laryngoscope*, 116(5):800–803.

Undurraga, J. A. (2013). *Basic neural mechanisms of the electrically stimulated auditory nerve*. PhD thesis, University of Leuven (KU Leuven).

Vermeire, K., Van de Heyning, P., et al. (2010). Better speech recognition in noise with the fine structure processing coding strategy. *ORL*, 72(6):305–311.

Wei, C.-G., Cao, K., and Zeng, F.-G. (2004). Mandarin tone recognition in cochlear-implant subjects. *Hearing research*, 197(1):87–95.

Wenger, C. (2012). *Human cochlear nerve model*. PhD thesis, TU Vienna.

Wilson, B. and Dorman, M. (2008a). Cochlear implants: Current designs and future possibilities. *J Rehabil Res Dev*, 45(5):695–730.

Wilson, B. S. (2004). Engineering design of cochlear implants. *Springer Handbook of Auditory Research*, 20:14–52.

Wilson, B. S. and Dorman, M. F. (2007). The surprising performance of present-day cochlear implants. *Biomedical Engineering, IEEE Transactions on*, 54(6):969–972.

Wilson, B. S. and Dorman, M. F. (2008b). Cochlear implants: A remarkable past and a brilliant future. *Hearing research*, 242(1):3–21.

Wilson, B. S., Finley, C. C., Lawson, D. T., Wolford, R. D., Eddington, D. K., and Rabinowitz, W. M. (1991). Better speech recognition with cochlear implants. *Nature*, 352(6332):236–238.

Zeng, F. (2004). Trends in cochlear implants. *Trends in amplification*, 8(1):1–34.

Zeng, F.-G., Rebscher, S., Harrison, W., Sun, X., and Feng, H. (2008). Cochlear implants: System design, integration, and evaluation. *Biomedical Engineering, IEEE Reviews in*, 1:115–142.

Zimmermann, C. E., Burgess, B. J., and Nadol Jr, J. B. (1995). Patterns of degeneration in the human cochlear nerve. *Hearing research*, 90(1):192–201.